2.2. Patients

Ninety-four consecutive patients (56 males, 38 females; range 28–88 years old, median 67.7 years) with primary NSCLC, who did not undergo preoperative chemo- and/or radiation therapy, were evaluated using our method (Table 1). Written informed consent was obtained from all patients enrolled. This study conformed to the ethical guidelines of Osaka University Graduate School of Medicine, and was approved by the institutional review board of Osaka University Medical Hospital. All patients underwent a segmentectomy ($n = 11$), lobectomy ($n = 80$), or bilobectomy ($n = 3$) with a systematic mediastinal lymphadenectomy from August 2008 to January 2010 at Osaka University Medical Hospital.

The postoperative staging of all patients was determined according to the tumor–node–metastasis (TNM) classification of the Union for International Cancer Control (UICC), ver. 7, 2009 (Table 1). The median follow-up duration was 13 months (6–22 months). In follow-up examinations, all patients were evaluated at 3-month intervals. Each evaluation included a physical examination, chest X-ray, and blood tests including tumor markers, while additional thoracic–abdominal computed tomography (CT) scans were generally performed at 6-month intervals.

2.3. Blood samples and ITC detection and enrichment

All blood samples were collected on the back table immediately after lung resection by gentle aspiration with an 18-gauge needle from the tumor-draining pulmonary vein (PV), which was stapled before the resection in all cases, and placed in 10-ml ethylene diamine tetraacetic acid (EDTA) tubes. ITCs were isolated using a negative selection method from 1-ml blood samples by the method described above. In addition, cytokeratin immunohistochemistry was performed, if an additional blood sample was available.

2.4. Evaluation and classification of clusters

Using all of the samples, one glass slide containing enriched ITCs from each patient was prepared and assessed by Papanicolaou staining. This examination was performed independently by two cytologists (E.Y and H.Y) who were unaware of the patient's clinical data. For morphological assessment, each cytologist distinguished cancer cells from normal cells by light microscopy based on their morphological appearance, such as cell size and shape, nuclear size and shape, and nuclear–cytoplasmic ratio (N/C). Furthermore, for cluster formation assessment, patterns of ITCs were classified into the following four types: no tumor cells (N), singular cells (S), clustered cells ($\leq$0.2 mm in size) (CSs) including singular cells, and bulky clustered cells (>0.2 mm in size) (BCSs), which included clustered cells and singular cells.

2.5. Statistical analysis

Statistical analysis was performed using the SPSS Exact Tests software. The Kruskal–Wallis test was used to calculate mean values, and prevalence was analyzed with Fisher's exact test. For analysis of follow-up data, survival curves were calculated with the Kaplan–Meier method and survival distributions were compared by a log-rank test. The Cox proportional hazards model was applied for calculating hazard ratio by uni- and multivariate analyses. The threshold for statistical significance was a p-value less than 0.05.

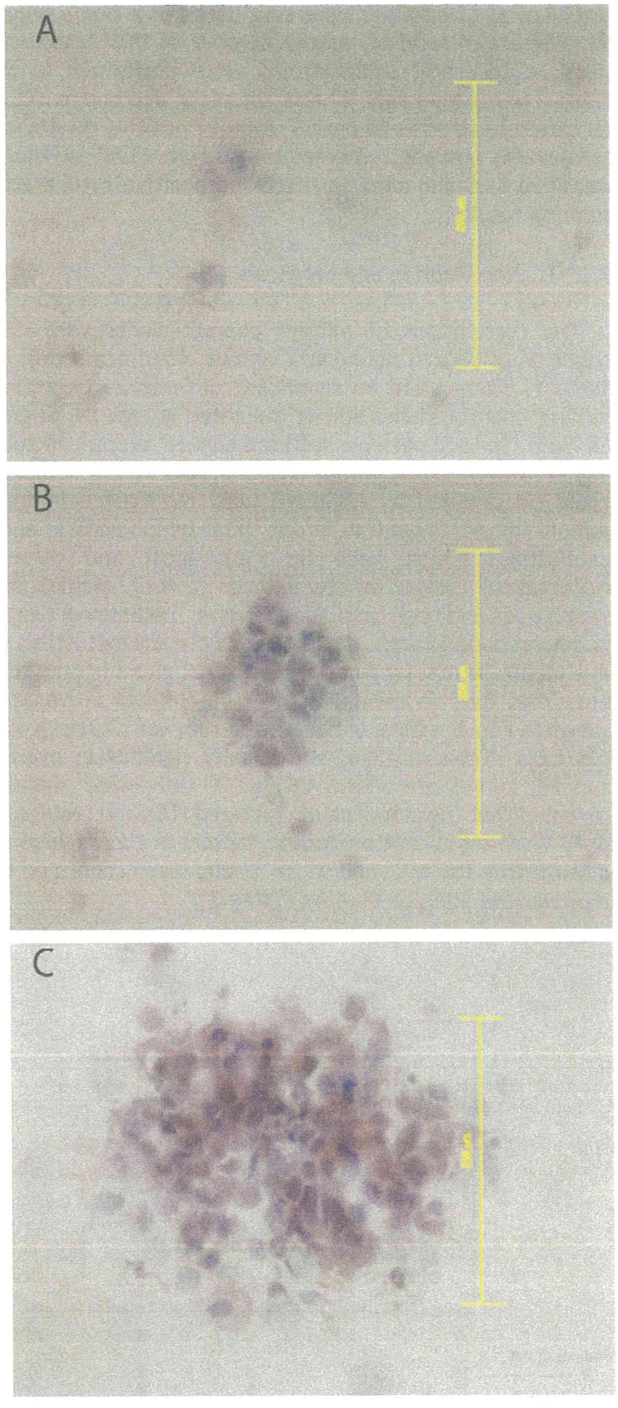

Fig. 1. Classification of isolated tumor cells by cluster formation. Shown are results following Papanicolaou staining. (A) Arrows indicate singular cancer cells. (B) Clustered cancer cells ($\leq$0.2 mm). (C) Bulky clustered cells (>0.2 mm). Original magnification ×40. Scale bars = 0.2 mm.

3. Results

3.1. Detection of ITCs

Using Papanicolaou staining, ITCs classified as S were detected in 33 (35%) of the 94 patients, while those classified as CS or BCS were found in 35 (37%). Fig. 1 shows examples of singular and cluster formations of CTCs. Cases classified as CS and BCS were considered as a single group for analysis of survival, as the number of BCS cases was small. Cytokeratin examinations were performed in 59 cases (15 classified as N, 21 as S, 22 as CS, and one as BCS). All cases classified as CS or BCS revealed positive results for cytokeratin staining, whereas only seven (33%) of those classified as S and none as N showed positive cytokeratin staining results.

3.2. ITC classification and prognosis

The correlations of patient characteristics with distribution of ITCs in pulmonary venous blood are shown in Table 1. There were no significant differences regarding patient characteristics among the three groups (N, S, and CS/BCS). Sixteen patients suffered cancer relapse, including 14 in the CS/BCS group, one in S, and one in N: these could be detailed as exclusive local recurrence in four (pleura in one, chest wall in one, hilar lymph node in one, mediastinal lymph node in one), local and distant metastasis in seven (bilateral lungs in four, mediastinal lymph node and neck lymph node in two, mediastinal lymph node and bone in one), and exclusive distant metastasis in five (contralateral lung in three, adrenal gland in one, and brain and liver in one). Relapse-free survival curves are shown in Fig. 2, which demonstrated that the cluster group (CS/BCS) exclusively was statistically significant; overall survival curves are shown in Fig. 3. Univariate analysis revealed that the presence of clustered ITCs and p-stage III or IV were significant prognostic factors in the analysis of disease-free survival, and those results were confirmed by multivariate analysis findings (Table 2).

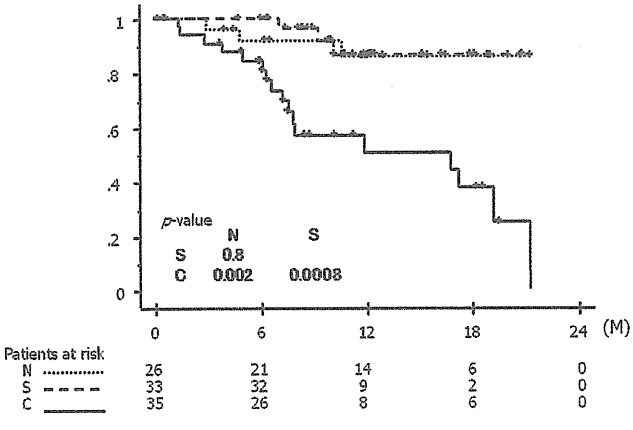

Fig. 2. Relapse-free survival curves.
N, patients with no tumor cells; S, patients with singular tumor cells; C, patients with clustered tumor cells (CS/BCS).

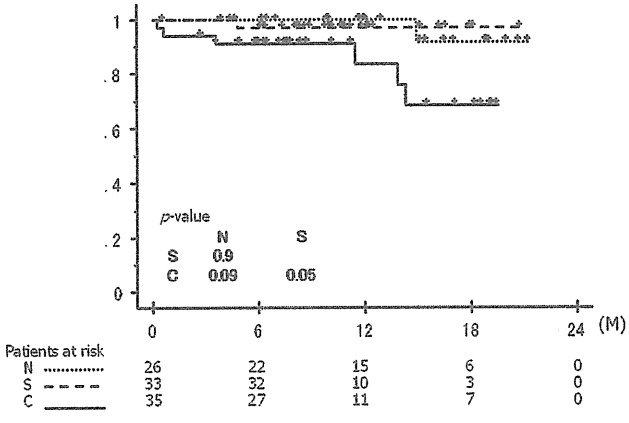

Fig. 3. Overall survival curves.
N, patients with no tumor cells; S, patients with singular tumor cells; C, patients with clustered tumor cells (CS/BCS).

4. Discussion

In the present study, we focused on the morphological appearance of ITCs and investigated related clinical implications. Our results showed that cluster formations of ITCs may be a prognostic indicator for early recurrence of lung cancer. In cases with singular cancer cells, the recurrence rate was low as compared with those with cluster formation. However, the clinical implications of the presence of singular ITCs remain unclear and a longer duration follow-up study is needed to determine clinical outcomes over a long period.

In spite of early discovery of cancer and complete surgical resection, the rates of recurrence and mortality in lung cancer cases remain high [1]. During treatment of postoperative patients, it is especially important to detect early relapse and distant metastasis. Thus, it is crucial to develop useful biomarkers for predicting early recurrence and metastasis. Some recent studies have demonstrated that the presence of ITCs in circulating blood was useful as a biomarker for the prognosis of various types of disease, such as breast cancer [7], colorectal cancer [6], and lung cancer [11].

Various methods to detect and enrich ITCs have been reported. In older studies, ITCs were observed using whole blood samples [12], though those results are not considered to be reliable. Recently, Sienel et al. used a cytokeratin immunohistochemistry method to reveal that the presence of ITCs in samples collected from the PV of a pulmonary lobe containing lung cancer before resection was a predictor of poor survival [13]. In addition, Yamashita et al. reported a study that used reverse transcriptase-polymerase chain reaction (RT-PCR) assays of peripheral blood to detect messenger RNA (mRNA) of carcinoembryonic antigen (CEA), and noted that its presence was a prognostic indicator in patients with NSCLC [11]. Current advancement in technology allow for ITCs to be captured and quantitatively evaluated with the semi-automated CellSearch® System (Veridex LLC, NJ, USA). Using this system, some groups have reported that determination of the number of pre- and postoperative ITCs was useful as a biomarker for survival and prognosis [7,10], while another showed that those results were able to reveal cancer cell spreading caused by the operation [14]. However, most of those studies used

Table 2. Results of univariate and multivariate analyses of relapse-free survival.

Variables	Univariate			Multivariate		
	R.R.	95% C.I.	*p*-Value	R.R.	95% C.I.	*p*-Value
ITCs in PV						
None	Ref.			Ref.		
Singular	0.901	0.180–4.505	0.9	0.845	0.170–4.577	0.9
Clustered	5.894	1.717–20.23	0.005	8.882	1.676–21.04	0.006
Gender						
Male	Ref.					
Female	0.882	0.355–1.904	0.7	0.895	0.319–2.515	0.8
Age in years						
<70	Ref.					
≥70	1.923	0.831–4.446	0.1	1.279	0.490–3.339	0.6
p-Stage						
I	Ref.					
II	2.122	0.686–6.557	0.2	2.096	0.588–7.474	0.3
III or IV	7.591	2.612–22.06	0.0002	9.756	3.357–40.37	0.002
Tumor histology						
Adenocarcinoma	Ref.					
Squamous cell carcinoma	1.717	0.560–5.265	0.3	2.147	0.588–7.847	0.2
Miscellaneous	2.456	0.806–7.482	0.1	1.081	0.225–5.204	0.9

quantitative evaluation methods and few have shown the significance of qualitative evaluation of ITCs.

In the present study, early relapse was associated with the presence of clustered cancer cells. We speculated that cancer cells may be able to live for a longer period in circulating blood when clustered, thus allowing direct access to distant organs and easy establishment of a secondary tumor. In addition, when considering tumor-initiating cells, it is possible that cells with a large diameter have a greater potential of causing relapse [15].

A recent study noted that epithelial–mesenchymal transition (EMT) plays important roles in cancer progression and metastasis [16]. Through the EMT process, the morphology and gene expression of the epithelial markers E-cadherin and cytokeratin become altered in cancer cells [17,18]. Our present analysis using immunohistochemical staining for cytokeratin showed that the positive rate of CS/BCS cases was 100%, whereas that in cases classified as S was low (33%). The reason for the different rates of positivity between S and CS/BCS cases may be related to EMT. Furthermore, the low occurrence of cytokeratin staining in cases classified as S may indicate that the expression of cytokeratin was reduced during the EMT process.

There are some limitations to our method, as accurate cell counting and ITC enrichment have not been perfected. On the other hand, with the CellSearch® system [7–10], cell-number counting and enrichment are easily performed in a semiautomatic fashion, though it is difficult to detect morphological features, in contrast to the method used in the present study. Moreover, there are problems with the procedure used to collect the samples. In the present method, in patients, after resecting the lung and placing it on the back table, blood was collected by aspiration from the PV, which had been stapled before the resection. Ideally, blood samples should be collected from the PV with proximal clamping before lung resection. In addition, it would be good to perform the assays with blood samples obtained from the peripheral vein. Some studies have presented preoperative and postoperative analyses of ITCs obtained from peripheral blood samples [7,11]. In the future, we intend to collect blood samples before lung resection and perform the assays using peripheral blood samples. In addition, we hope to conduct additional research using blood samples obtained at various time points before, during, and after surgery.

In conclusion, the present CD45-negative selection method was found useful to detect and enrich ITCs from blood samples obtained from the PV of lungs resected for NSCLC. In addition, our results show the clinical relevance of morphological classification of ITCs in NSCLC cases, as the presence of clustered ITCs was a prognostic indicator for patients following surgical resection.

Acknowledgments

The authors thank Professor Katsuyuki Aozasa, Dr Eiichi Morii, and Dr Hideo Yoshimura (Department of Pathology, Osaka University Graduate School of Medicine) for their contributions to the cytological diagnosis.

References

[1] Alberg AJ, Ford JG, Samet JM. American College of Chest Physicians. Epidemiology of lung cancer: ACCP evidence-based clinical practice guidelines (2nd edition). Chest 2007;132:29S–55S.
[2] Pantel K, Brakenhoff RH, Brandt B. Detection, clinical relevance and specific biological properties of disseminating tumour cells. Nat Rev Cancer 2008;8:329–40.
[3] Smith B, Selby P, Southgate J, Pittman K, Bradley C, Blair GE. Detection of melanoma cells in peripheral blood by means of reverse transcriptase and polymerase chain reaction. Lancet 1991;338:1227–9.
[4] Kurusu Y, Yamashita J, Ogawa M. Detection of circulating tumor cells by reverse transcriptase-polymerase chain reaction in patients with resectable non-small-cell lung cancer. Surgery 1999;126:827–8.
[5] Iinuma H, Okinaga K, Egami H, Mimori K, Hayashi N, Nishida K, Adachi M, Mori M, Sasako M. Usefulness and clinical significance of quantitative real-time RT-PCR to detect isolated tumor cells in the peripheral blood and tumor drainage blood of patients with colorectal cancer. Int J Oncol 2006;28:297–306.
[6] Ignatiadis M, Xenidis N, Perraki M, Apostolaki S, Politaki E, Kafousi M, Stathopoulos EN, Stathopoulou A, Lianidou E, Chlouverakis G, Sotiriou C, Georgoulias V, Mavroudis D. Different prognostic value of cytokeratin 19 mRNA positive circulating tumor cells according to estrogen receptor and HER2 status in early-stage breast cancer. J Clin Oncol 2007;25:5194–202.
[7] Okumura Y, Tanaka F, Yoneda K, Hashimoto M, Takuwa T, Kondo N, Hasegawa S. Circulating tumor cells in pulmonary venous blood of primary lung cancer patients. Ann Thorac Surg 2009;87:1669–75.

[8] Sastre J, Maestro ML, Puente J, Veganzones S, Alfonso R, Rafael S, Garcia-Saenz JA, Vidaurreta M, Martin M, Arroyo M, Sanz-Casla MT, Diaz-Rubio E. Circulating tumor cells in colorectal cancer: correlation with clinical and pathological variables. Ann Oncol 2008;19:935–8.
[9] Cristofanilli M, Budd GT, Ellis MJ, Stopeck A, Matera J, Miller MC, Reuben JM, Doyle GV, Allard WJ, Terstappen LW, Hayes DF. Circulating tumor cells, disease progression, and survival in metastatic breast cancer. N Engl J Med 2004;351:781–91.
[10] Tanaka F, Yoneda K, Kondo N, Hashimoto M, Takuwa T, Matsumoto S, Okumura Y, Rahman S, Tsubota N, Tsujimura T, Kuribayashi K, Fukuoka K, Nakano T, Hasegawa S. Circulating tumor cell as a diagnostic marker in primary lung cancer. Clin Cancer Res 2009;15:6980–6.
[11] Yamashita J, Matsuo A, Kurusu Y, Saishoji T, Hayashi N, Ogawa M. Preoperative evidence of circulating tumor cells by means of reverse transcriptase-polymerase chain reaction for carcinoembryonic antigen messenger RNA is an independent predictor of survival in non-small cell lung cancer: a prospective study. J Thorac Cardiovasc Surg 2002;124:299–305.
[12] Stuart R, Alvin W, Ruth M, Elizabeth M, Warren C. Technique and results of isolation of cancer cells from the circulating blood. AMA Arch of Surg 1958;76:334–46.
[13] Sienel W, Seen-Hibler R, Mutschler W, Pantel K, Passlick B. Tumour cells in the tumour draining vein of patients with non-small cell lung cancer: detection rate and clinical significance. Eur J Cardiothorac Surg 2003;23:451–6.
[14] Sawabata N, Okumura M, Utsumi T, Inoue M, Shiono H, Minami M, Nishida T, Sawa Y. Circulating tumor cells in peripheral blood caused by surgical manipulation of non-small-cell lung cancer: pilot study using an immunocytology method. Gen Thorac Cardiovasc Surg 2007;55:189–92.
[15] Liotta LA, Kleinerman J, Saidel GM. Quantitative relationships of intravascular tumor cells, tumor vessels, and pulmonary metastases following tumor implantation. Cancer Res 1974;34:997–1004.
[16] Thiery JP, Acloque H, Huang RY, Nieto MA. Epithelial-mesenchymal transitions in development and disease. Cell 2009;139:871–90.
[17] Tsuji T, Ibaragi S, Hu GF. Epithelial-mesenchymal transition and cell cooperativity in metastasis. Cancer Res 2009;69:7135–9.
[18] Koo V, El Mekabaty A, Hamilton P, Maxwell P, Sharaf O, Diamond J, Watson J, Williamson K. Novel in vitro assays for the characterization of EMT in tumourigenesis. Cell Oncol 2010;32:67–76.

Appendix A. Conference discussion

Dr G. Varela (Salamanca, Spain): To my knowledge, you are the first to demonstrate that the presence of clusters of tumor cells in pulmonary venous blood adversely influences the prognosis in pathological stage I non-small cell lung cancer cases.

Previously, different authors have reported the finding of epithelial cells in blood obtained from pulmonary veins after lung resection by means of antibodies against the epithelial cell adhesion molecule using the so-called Cell Search System. According to Passlick, this happens in less than 20% of the resected cases, while Okumura and co-workers reported circulating tumor cells in more than 95% of their cases. With your technique you have detected clusters of tumor cells in around 30% of your cases. This seems to be more specific for tumor cell detection and also more sensitive than simple immunohistochemical staining. I'm wondering if this 30% prevalence of clusters of cells may be related to anatomical conditions or to the type of surgical techniques; for instance, the tumor size or location in the lobe, the way of handling the tumor during surgery, the sequence of vessel ligation and so on.

My second question is, if the finding of clusters of cells is not related to surgical manipulation, maybe comparable findings could be elicited in sequentially-taken samples of peripheral arterial blood prior to surgery, indicating the need for induction chemotherapy even in selected clinical stage IA cases. Do you have any preliminary data on this or are you thinking about a similar study?

Dr Funaki: As you mentioned, I think surgical manipulation is an important problem. I think surgical manipulation may enhance the cancer cells shedding into the bloodstream, as you mentioned, but I don't think that all cancer cells are shed into the bloodstream only by surgical manipulation.

As for the surgical techniques, in our research we first ligate the pulmonary vein. So there is the possibility that surgical manipulation may enhance cancer cells shedding in the bloodstream and that the number of isolated tumor cells may increase.

UICC
global cancer control

IJC
International Journal of Cancer

Overexpression of SOCS3 exhibits preclinical antitumor activity against malignant pleural mesothelioma

Kota Iwahori[1,2], Satoshi Serada[1], Minoru Fujimoto[1], Shintaro Nomura[3], Tadashi Osaki[2], Chun Man Lee[4], Hiroyuki Mizuguchi[5], Tsuyoshi Takahashi[1], Barry Ripley[6], Meinoshin Okumura[7], Ichiro Kawase[2], Tadamitsu Kishimoto[6] and Tetsuji Naka[1]

[1] Laboratory for Immune Signal, National Institute of Biomedical Innovation, Osaka, Japan
[2] Department of Respiratory Medicine, Allergy, and Rheumatic Diseases, Osaka University Graduate School of Medicine, Osaka, Japan
[3] Faculty of Animal Bioscience, Nagahama Institute of Bio-Science and Technology, Shiga, Japan
[4] Medical Center for Translational Research, Osaka University Hospital, Osaka, Japan
[5] Laboratory of Gene Transfer and Regulation, National Institute of Biomedical Innovation, Osaka, Japan
[6] Laboratory of Immune Regulation, Osaka University Graduate School of Frontier Biosciences, Osaka, Japan
[7] Department of General Thoracic Surgery, Osaka University Graduate School of Medicine, Osaka, Japan

Malignant pleural mesothelioma (MPM) is an aggressive tumor with poor prognosis for which an effective therapy remains to be established. Our study investigated the therapeutic potential of the suppressor of cytokine signaling 3 (SOCS3), an endogenous inhibitor of intracellular signaling pathways, for treatment of MPM. We infected MPM cells (H226, EHMES-1, MESO-1 and MESO-4) with an adenovirus-expressing SOCS3 (AdSOCS3) to examine the effect of SOCS3 overexpression on MPM cells. SOCS3 overexpression reduced MPM proliferation and induced apoptosis and partial G0/G1 arrest. SOCS3 also inhibited the proliferation of MPM cells *via* multiple signaling pathways including Janus kinase (JAK)/signal transducer and activator of transcription 3 (STAT3), extracellular signal-regulated kinase (ERK), focal adhesion kinase (FAK) and p53 pathways. Notably, AdSOCS3 treatment inhibited tumor growth in an MPM pleural xenograft model. These findings demonstrate that overexpression of SOCS3 has a potent antitumor effect against MPM both *in vitro* and *in vivo* and indicate the potential for clinical use of SOCS3 for MPM treatment.

Malignant pleural mesothelioma (MPM) is an aggressive tumor arising from the mesothelial cells of serosal cavities. MPM may be asymptomatic at the early stage and is sometimes observed incidentally during routine chest radiography. Common symptoms include chest pain and dyspnea, which are caused by tumor invasion of the chest wall or pleural effusion and occur late during disease progression. Although chemotherapy with the drug pemetrexed improves survival time for unresectable MPM patients, the overall median survival time is only 12 months.[1] MPM is often associated with past exposure to asbestos, in which case there is a long latency period, often exceeding 20 years, between first exposure to asbestos and diagnosis of MPM.[2] The number of deaths from MPM is expected to increase in the next 20 years world-wide where heavy use of asbestos has occurred.[2–5] There is thus a growing need for the development of new therapies to treat this disease.

A growing number of studies of MPM tumor biology have established important roles for cytokines involved in tumor growth or the spread of this disease.[6–10] A reported potential molecular target for MPM therapeutics is the interleukin-6 (IL-6)/Janus kinase (JAK)/signal transducer and activator of transcription 3 (STAT3) signaling pathway and

Key words: malignant pleural mesothelioma, suppressor of cytokine signaling 3, gene therapy, signal transducer and activator of transcription 3, p53

Abbreviations: 7-AAD: 7-amino-actinomycin D; DAPI: 4′,6-diamidino-2-phenylindole; DMSO: dimethyl sulfoxide; ERK: extracellular signal-regulated kinase; FAK: focal adhesion kinase; FCS: fetal calf serum; IL-6: interleukin-6; JAK: Janus kinase; MPM: malignant pleural mesothelioma; MOI: multiplicity of infection; MRA: anti-IL-6 receptor antibody; MTS: 3-(4,5-dimethylthiazol-2-yl)-5-(3-carboxymethoxyphenyl)-2-(4-sulfophenyl)-2H-tetrazolium; pfu: plaque-forming units; PI: propidium iodide; SH2: Src homology 2; SHP: SH2-domain-containing tyrosine phosphatase; siRNA: small interfering RNA; SOCS3: suppressor of cytokine signaling 3; STAT3: signal transducer and activator of transcription 3; TUNEL: Terminal deoxynucleotidyl transferase-mediated dUTP nick-end labeling

Grant sponsor: Ministry of Health, Labour and Welfare, Japan, Ministry of Education, Culture, Sports, Science and Technology, Japan
DOI: 10.1002/ijc.25716
History: Received 15 Jun 2010; Accepted 22 Sep 2010; Online 14 Oct 2010
Correspondence to: Tetsuji Naka, Laboratory for Immune Signal, National Institute of Biomedical Innovation, 7-6-8 Saito-Asagi, Ibaraki, Osaka 567-0085, Japan, Tel.: +81-72-641-9843, Fax: +81-72-641-9837, E-mail: tnaka@nibio.go.jp

high-level expression of IL-6 in the pleural fluid of MPM patients.[11,12] The binding of IL-6 to its cognate receptor leads to a conformational change in the receptor that initiates the activation of JAK, which in turn activates the transcription factor STAT3 to dimerize and translocate into the nucleus, thus leading to the initiation of target gene transactivation. This pathway is crucial for the occurrence of hematopoiesis, immune response and oncogenesis.[13] Moreover, dysfunction of the regulatory system for the JAK/STAT3 pathway has been demonstrated to be involved in the development of cancer.[13]

The suppressor of cytokine signaling (SOCS) family proteins[14–16] participate in the negative regulation of multiple signaling pathways including the IL-6/JAK/STAT3 signaling pathway,[17–19] while SOCS3 can bind both the cytokine receptor and JAK, thus facilitating inhibition of the JAK molecule.[20] The restoration of SOCS3 expression in several cancer cell lines was found to effectively suppress tumorigenicity.[21] Because the JAK/STAT3 signaling pathway is frequently activated in a wide variety of human malignancies,[22] SOCS3 gene delivery may represent a novel therapeutic strategy for the treatment of human cancers, including mesothelioma.

In addition to the IL-6/JAK/STAT3 signaling pathway, various other signaling pathways are associated with tumorigenesis in MPM. Among these pathways, activators of oncogenic molecules such as the extracellular signal-regulated kinase (ERK) and focal adhesion kinase (FAK) have been implicated.[23,24] It was reported that SOCS3 participated in the inhibition of ERK phosphorylation and the degradation of FAK.[25–27] SOCS3 can competitively block receptor recruitment of SH2-domain-containing tyrosine phosphatase (SHP-2) to Tyr759 of gp130, thus inhibiting ERK activation. Interactions of SOCS3 with FAK through the Src homology 2 (SH2) domain have been reported to promote polyubiquitination and subsequent degradation of FAK. Because there are multiple abnormalities in signal transduction and genetic differences in individual patients, SOCS3, which, as seen above, is involved in the regulation of multiple signals, is expected to be effective for the treatment of MPM. However, the potential therapeutic benefits of SOCS3 for MPM have not yet been investigated. In the study presented here, we investigated the efficacy of SOCS3 gene delivery for the treatment of MPM.

Material and Methods

Cell lines

Mesothelioma cell lines H28, H226 and H2452 were purchased from American Type Culture Collection (Manassas, VA). Mesothelioma cell line EHMES-1 was kindly provided by Dr. Hironobu Hamada (Ehime University, Ehime, Japan). ACC-MESO-1 (MESO-1) and ACC-MESO-4 (MESO-4) cell lines were purchased from RIKEN BRC cell bank (Tsukuba, Japan). All the cells were cultured in RPMI 1640 (Wako, Osaka, Japan) with 10% fetal calf serum (FCS) (HyClone Laboratories, Logan, UT), 100 IU/mL penicillin and 100 μg/mL streptomycin (Nacalai Tesque, Kyoto, Japan). Human adult mesothelial cells were purchased from Zen-Bio (Research Triangle Park, NC) and cultured in Mesothelial Cell Growth Medium (Zen-Bio). HEK293 cells were obtained from the JCRB Cell Bank (Tokyo, Japan) and cultured in DMEM (Wako) with 10% FCS (HyClone), 100 IU/mL penicillin and 100 μg/mL streptomycin (Nacalai Tesque).

Reagents

Recombinant human IL-6 was kindly provided by Dr. Kazuyuki Yoshizaki (Osaka University, Osaka, Japan), recombinant soluble IL-6 receptor (sIL-6R) and anti-IL-6R monoclonal antibody (tocilizumab, currently known as MRA) were obtained from Chugai Pharmaceutical Co. (Tokyo, Japan). Purified human IgG, purchased from Sigma (St. Louis, MO), was used as control for MRA. JAK inhibitor I and PD98059 were purchased from Calbiochem (La Jolla, CA) and doxorubicin from Wako.

Preparation of adenoviruses

Replication-defective recombinant adenoviral vectors were constructed with the cosmid–adenoviral DNA terminal protein complex method.[28] Adenoviral vectors AdLacZ and adenovirus-expressing SOCS3 (AdSOCS3) were designed to express the LacZ gene and the human SOCS3 gene, respectively, under the control of the CAG promoter (a modified chicken β-actin promoter with a cytomegalovirus immediate early enhancer).[29–31] Solutions of these adenoviral vectors were prepared as described previously and stored at −80°C until use.[32] Adenoviral vectors containing the genes for HA-tagged Y705F dominant-negative STAT3 (AddnSTAT3) were kindly provided by Dr. Akihiko Yoshimura (Keio University, Tokyo, Japan).

X-gal staining

The transduction efficiency of adenoviral vectors was assessed by means of X-gal staining. Cells were cultured in 6-well plates at a density of 1×10^5 cells per well and infected with AdLacZ at the indicated multiplicities of infection (MOIs). X-gal staining was performed 24 hr after infection according to the protocol provided by the manufacturer (Sigma-Aldrich, St. Louis, MO).

Reverse transcription-polymerase chain reaction analysis

Total RNA of cultured cells was isolated with Sepasol-RNA I (Nacalai Tesque) and cDNAs were synthesized from 500 ng of each total RNA preparation with a Quantitect Reverse Transcription kit (QIAGEN, Valencia, CA), all according to the manufacturers' instructions. The TaKaRa Ex Taq (Takara Bio, Otsu, Shiga, Japan) was used for reverse transcription-polymerase chain reaction (RT-PCR) analysis. β-actin was used as a housekeeping gene to evaluate and compare the quality of different cDNA samples. Primers for β-actin (67°C annealing, 33 cycles) were: forward, 5′-AGCCTCGCCTTTGCCGA-3′;

reverse, 5′-CTGGTGCCTGGGGCG-3′. Primers for SOCS3 (55°C annealing, 33 cycles) were: forward, 5′-TCAAGACCTT-CAGCTCCAAG-3′; reverse, 5′-TTGACGCTGAGCGTGAAGAA-3′. And primers for p53 (60°C annealing, 33 cycles) were: forward, 5′-CCCCAGCCAAAGAGAAACC-3′; reverse, 5′-TCCAAGGCCTCATTCAGCTCT-3′. PCR products were detected by means of 1% agarose gel electrophoresis with ethidium bromide staining.

Small interfering RNA transfection

Commercial JAK1 small interfering RNA (siRNA) was obtained from QIAGEN. Cells were transfected with siRNA using Lipofectamine 2000 reagent (Invitrogen, Carlsbad, CA) according to the manufacturer's instructions. Nonspecific siRNA (QIAGEN) was used as a negative control, and the selective silencing of JAK1 was confirmed by Western blot analysis.

Measurement of IL-6 and sIL-6R concentrations in culture supernatant

MPM cells were cultured in 6-well plates at a density of 1×10^5 cells per well and incubated in RPMI 1640 medium containing 0.5% FCS. The concentrations of IL-6 and sIL-6R in the 24-hr culture supernatant were measured by means of Quantikine Colorimetric Sandwich ELISA (R&D Systems, Minneapolis, MN).

SDS-PAGE and western blot analysis

Whole cell protein extract was prepared from MPM cells in RIPA buffer [10 mmol/L Tris-HCl (pH 7.5), 150 mmol/L NaCl, 1% (v/v) NP-40, 0.1% (w/v) SDS, 0.5% (w/v) sodium deoxycholate, 1 mmol/L Na_3VO_4, and 1× protease inhibitor cocktail (Roche Applied Science, Indianapolis, IN)]. Extracted proteins were resolved on SDS-PAGE and transferred to an Immobilon-P Transfer membrane (Millipore, Bedford, MA). The following antibodies were used: antiphospho-STAT3, 1:1,000; anticleaved caspase-3, 1:500; antiphospho-ERK, 1:1,000; anti-ERK, 1:1,000; antiphospho-p53 (Ser46), 1:1,000; antiphospho-p53 (Ser392), 1:1,000 (all from Cell Signaling Technology, Danvers, MA), anti-STAT3, 1:1,000; anti-p53, 1:500; anti-GAPDH, 1:1,000 (all from Santa Cruz Biotechnology, Santa Cruz, CA), antiphospho-FAK (Tyr397) (1:1,000; Biosource, Camarillo, CA), anti-JAK1, 1:1,000; anti-FAK, 1:1,000, anti-p21, 1:1,000 (all from BD Transduction Laboratories, San Jose, CA), antiphosphotyrosine (clone 4G10), 1:1,000 (Upstate Biotechnology, Lake Placid, NY) and anti-SOCS3 antibody (1:500; IBL, Gunma, Japan), followed by a 1:5,000 dilution of donkey antirabbit or 1:5,000 dilution of sheep antimouse horseradish peroxidase-conjugated secondary antibodies (GE Healthcare Bio-Sciences, Piscataway, NJ) and visualized with the Western Lightning ECL reagent (Perkin-Elmer, Boston, MA).

Immunoprecipitation

Cells were lysed in ice-cold RIPA buffer. After clearing of the lysate, anti-p53 antibody (Cell Signaling Technology) was added to the lysate followed by overnight incubation at 4°C. Protein G Sepharose (GE Healthcare Bio-Sciences) was then added and incubated by end-over-end mixing for 2 hr. The beads were washed five times in RIPA buffer and analyzed by Western blotting.

Phospho-kinase array

Expression of phosphorylated proteins was detected with the Proteome Profiler™ Human Phospho-Kinase Array kit (R&D Systems). The procedures were performed according to the manufacturer's protocol using 400 μg protein lysate per array.

MTS assay

MPM cell lines were plated in 96-well plates at a density of 1,000 cells per well and incubated in RPMI 1640 medium containing 10% FCS. After a three-day culture, cell proliferation was evaluated with the 3-(4,5-dimethylthiazol-2-yl)-5-(3-carboxymethoxyphenyl)-2-(4-sulfophenyl)-2H-tetrazolium (MTS) assay (CellTiter 96 aqueous nonradioactive cell proliferation assay; Promega, Madison, WI). MTS color development was measured and analyzed with a microplate reader Model 680 (Bio-Rad Laboratories, Hercules, CA) at a wavelength of 450 nm with a reference wavelength of 750 nm. This assay was performed in triplicate.

Apoptosis assay

MPM cells were grown to confluence to attain synchronization in G1 and subcultured at a lower density (1×10^5 cells in a six-well plate) for 24 hr so that most of the cells were in the S phase. Adenoviral vectors were infected by distributing suspensions of AdSOCS3 or AdLacZ onto cells at a MOI of 40, followed by incubation at 37°C for an additional 72 hr. The cells were then trypsinized and collected with the supernatants, followed by determination of cell viability by means of annexin V and 7-amino-actinomycin D (7-AAD) staining (BD Biosciences, San Jose, CA) using the FACSCanto flow cytometer (BD Biosciences). Data were analyzed with FlowJo software (Tree Star, Ashland, OR). This assay was performed in duplicate.

Cell cycle assay

MPM cells were grown to confluence to attain synchronization in G1 and subcultured at a lower density (1×10^5 cells in a six-well plate) for 24 hr so that most of the cells were in the S phase. Adenoviral vectors were infected by distributing suspensions of AdSOCS3 or AdLacZ onto cells at an MOI of 40, followed by incubation at 37°C for an additional 24 hr. The cells were then trypsinized and collected with the supernatants, after which the cell cycle was determined by means of propidium iodide (PI) staining according to the instructions for the Cycle Test Plus DNA Reagent kits (BD Biosciences) using the FACSCanto flow cytometer. This assay was performed in duplicate.

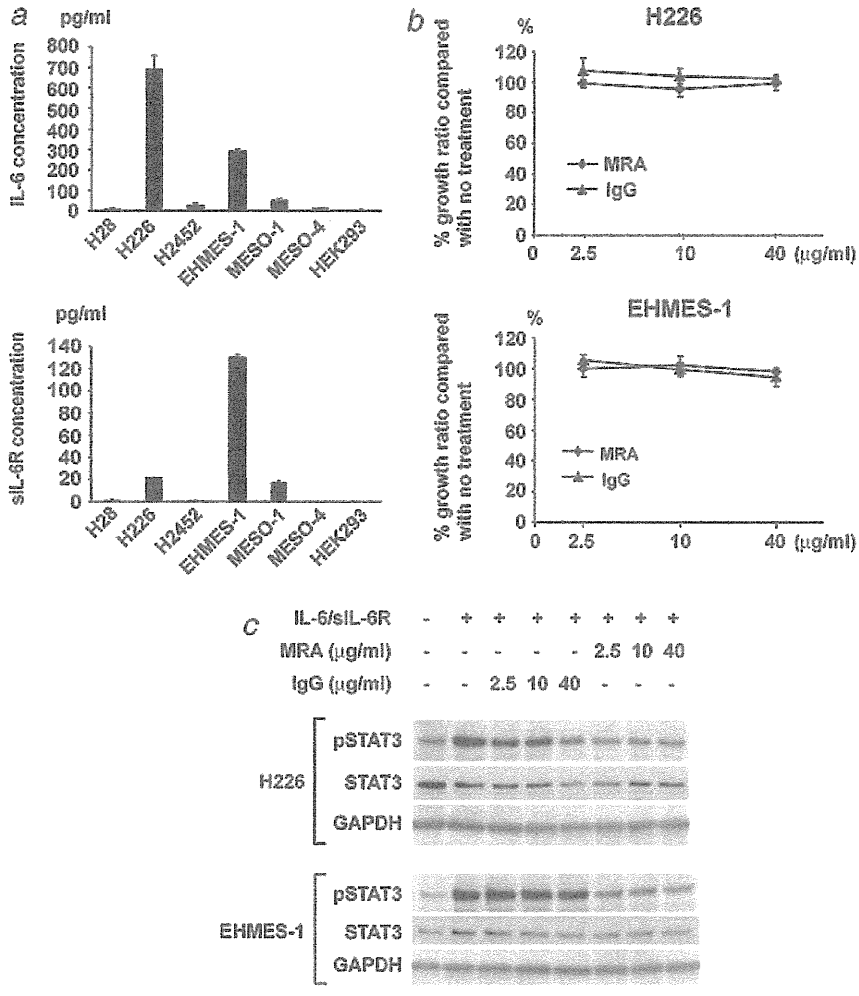

Figure 1. MRA treatment does not inhibit the growth of MPM cells. (*a*) IL-6 and sIL-6R concentrations were measured by using sandwich ELISA. Results are shown as average (columns) + SD (bars). (*b*) Growth curves of H226 and EHMES-1 cells treated with MRA. Cells were cultured in RPMI medium containing 10% FCS with 2.5–40 μg/mL MRA or human IgG. After a 3-day culture, viable cell numbers were counted with the MTS assay. Figures show the average (points) of triplicate wells ± SD (bars). (*c*) Inhibition of phosphor-STAT3 by MRA. H226 and EHMES-1 cells were cultured in RPMI medium containing 0.5% FCS with 2.5–40 μg/mL MRA or human IgG. After a 24-hr culture, the phosphorylation of STAT3 in MPM cells was analyzed after 10-min stimulation with 100 ng/mL of IL-6 and 100 ng/mL of sIL-6R. The lysates from IL-6- and sIL-6R-stimulated cells were analyzed by means of Western blot with antiphospho STAT3 antibody, and subsequently with anti-STAT3 and anti-GAPDH antibody.

Mouse xenograft model

All animal experiments were conducted according to the institutional ethical guidelines for animal experimentation of the National Institute of Biomedical Innovation (Osaka, Japan). Female ICR *nu/nu* mice, 6 to 7 weeks of age, were obtained from Charles River Japan (Yokohama, Japan). The mice were housed for 7 to 14 days and allowed *ad libitum* access to food and water.

For subcutaneous xenograft experiments, we injected 3×10^6 cells in a total volume of 100 μL of 1/1 (v/v) PBS/Matrigel (Becton Dickinson, Bedford, MA) in the flank of ICR *nu/nu* mice. When the tumor sizes reached ~100 mm^3, 1×10^8 plaque-forming units (pfu)/50 μL of AdSOCS3 or AdLacZ was injected intratumorally twice per week. Tumor volumes were determined weekly by measuring in two dimensions, length (L) and width (W), and calculating volume as $(W^2 \times L)/2$.

For pleural xenograft experiments, cells were resuspended in PBS at a density of 1×10^6 cells in a total volume of 150 μL of 1/1 (v/v) PBS/Matrigel (Becton Dickinson). The mice were intrathoracically injected with 150 μL of the cell suspension through a 26-gauge needle. Seven, 14 and 21 days after cell inoculation, 5.0×10^7 plaque-forming units (pfu)/

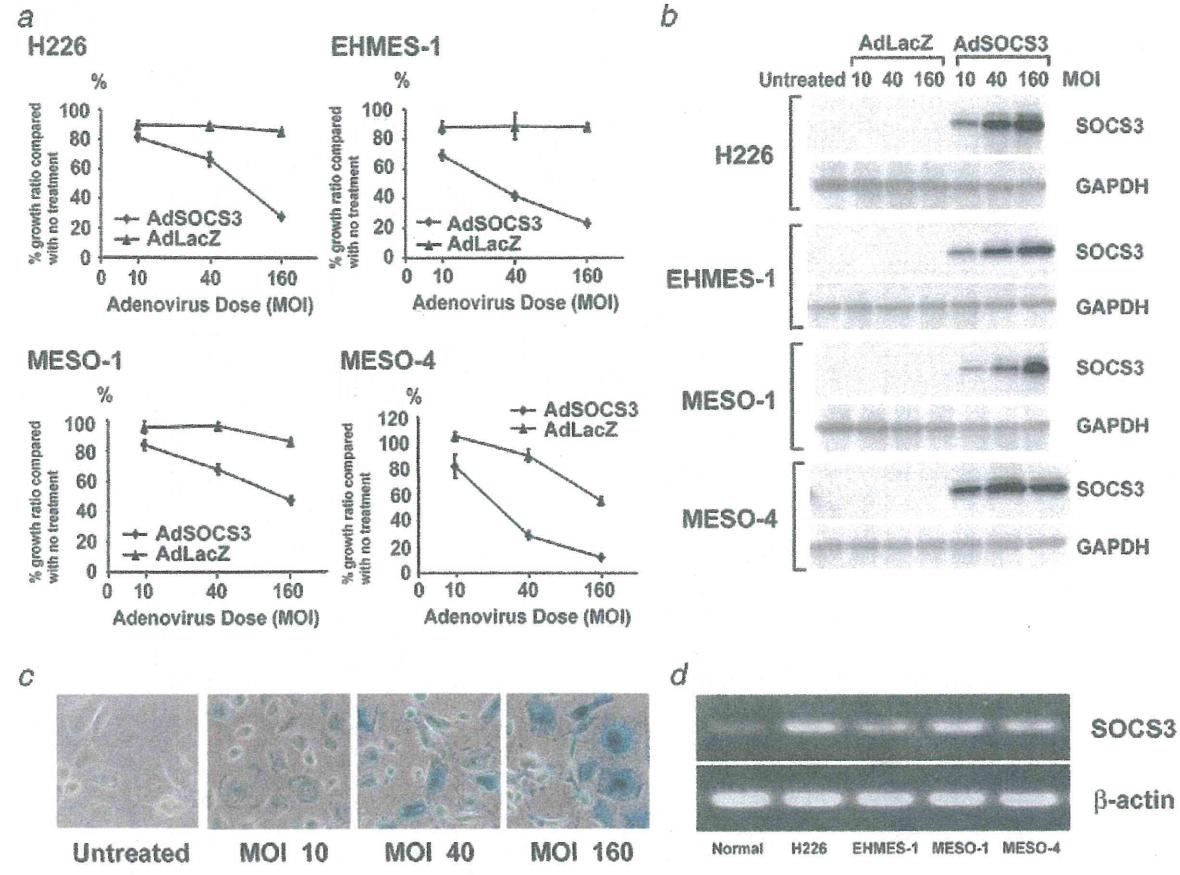

Figure 2. Overexpression of SOCS3 inhibits the growth of MPM cells. (*a*) Growth curves of MPM cells treated with AdSOCS3. Cells were infected with either AdSOCS3 or AdLacZ as control at an MOI of 10–160. Cells were cultured in RPMI 1640 medium containing 10% FCS. After a 3-day culture, viable cell numbers were counted with the MTS assay. Figures show the average (points) of triplicate wells ± SD (bars). (*b*) Expression of SOCS3 as a result of transduction of AdSOCS3. Cells were infected with either AdSOCS3 or AdLacZ as control at an MOI of 10–160. Cells were cultured in RPMI 1640 medium containing 10% FCS. After a 24-hr culture, the cell lysates were analyzed by means of Western blotting using anti-SOCS3 antibody and subsequently with anti-GAPDH antibody. (*c*) Transduction efficiency of the adenoviral vector in H226 cells. H226 cells were infected with AdLacZ at the indicated MOI and stained with X-gal 24 hr after infection. (*d*) Expression of endogenous SOCS3. RT-PCR was used for the assessment of SOCS3 expression.

150 μL of AdSOCS3 or AdLacZ was injected into the thoracic space with the same technique. Twenty-eight days after cell inoculation, the mice were sacrificed and their thoracic spaces examined macroscopically for growths, and tumors detected in the thoracic spaces were removed and weighed.

Immunohistochemistry

Tumors in the thoracic spaces were harvested and paraffin embedded for immunohistochemical analysis using anti-SOCS3 antibody (IBL). Terminal deoxynucleotidyl transferase-mediated dUTP nick-end labeling (TUNEL) assay (with DAPI nuclear counterstaining) for apoptosis was performed using the ApopTag® Fluorescein *in situ* Apoptosis Detection Kit (Chemicon International, Temecula, CA) according to the manufacturer's instructions.

Statistical analysis

Data are shown as mean ± SD for the number of experiments indicated. Student's *t*-test was used for comparison of the data. Differences were considered significant at $p < 0.05$.

Results

MRA treatment has no inhibitory effect on the growth of MPM cells

Reports of high-level expression of IL-6 in the pleural fluid of MPM patients prompted us to investigate the role of this signaling pathway in MPM. To characterize IL-6/sIL-6R levels secreted by MPM cell lines, we used sandwich ELISA for quantitation of IL-6/sIL-6R levels in 24-hr culture supernatants. As shown in Figure 1*a*, H226 and EHMES-1 were identified as cell lines with high IL-6/sIL-6R secretion.

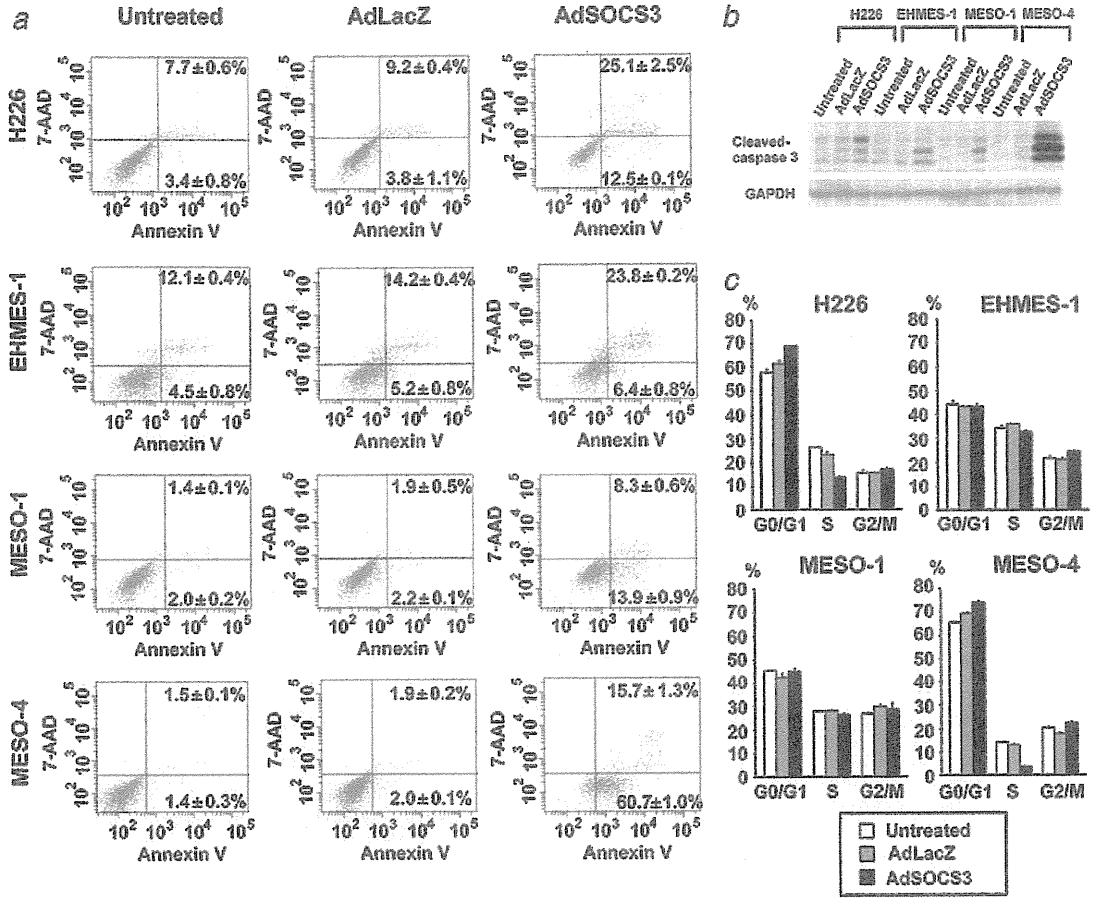

Figure 3. SOCS3 induces apoptosis and G0/G1 arrest in MPM cells. (*a*) Cells were infected with either AdSOCS3 or AdLacZ as control at an MOI of 40. Cells were cultured in RPMI 1640 medium containing 10% FCS for 3 days. Apoptosis was determined by means of annexin V and 7-AAD staining using flow cytometry. Figures show the average of duplicate wells ± SD. (*b*) Cells were infected with either AdSOCS3 or AdLacZ as control at an MOI of 40. Cells were cultured in RPMI 1640 medium containing 10% FCS for 3 days. Whole cell extracts were prepared and immunoblotted with anticleaved caspase-3 antibody. (*c*) Cells were infected with either AdSOCS3 or AdLacZ as control at an MOI of 40. Cells were cultured in RPMI 1640 medium containing 10% FCS for 24 hr. The cell cycle was determined by means of propidium iodide (PI) staining using flow cytometry. Figures show the average (columns) of duplicate wells + SD (bars).

Because it has been reported that IL-6 may represent a therapeutic target for tumorigenesis in MPM cells,[12] we subsequently tested the effect of anti-IL-6R monoclonal antibody (MRA) treatment. For this analysis, we used H226 and EHMES-1 cells which secrete high levels of IL-6. Figure 1*b* shows that MRA did not inhibit cell growth in H226 and EHMES-1 cells. On the other hand, it has been reported that 25 μg/mL of MRA is required for sufficient growth suppression of Lennert's lymphoma-derived T cells which show IL-6–dependent cell growth[12] and we demonstrated that MRA inhibited IL-6-stimulated STAT3 phosphorylation in MPM cells (Fig. 1*c*). These results suggest that, although H226 and EHMES-1 cells secreted high levels of IL-6, IL-6 signaling had little effect on the growth of these cells. However, the role of STAT3 on cell growth in H226 and EHMES-1 cells was not clear since MRA treatment did not inhibit endogenous phosphorylated STAT3 levels in these cells.

Overexpression of SOCS3 inhibits the growth of MPM cells

The JAK/STAT3 pathway is an important signaling pathway negatively regulated by SOCS3. We therefore used a replication-defective recombinant adenoviral vector to investigate the regulation of MPM cell growth by SOCS3. As shown in Figure 2*a*, AdSOCS3 strongly inhibited cell growth in H226, EHMES-1, MESO-1 and MESO-4 cells, while the endogenous SOCS3 expression levels of MPM cells were higher than those of normal mesothelial cells (Fig. 2*d*). This indicates that overexpression of SOCS3 was required for growth inhibition of MPM cells. Because sufficient transduction efficiency of the adenovirus vector and strong expression of

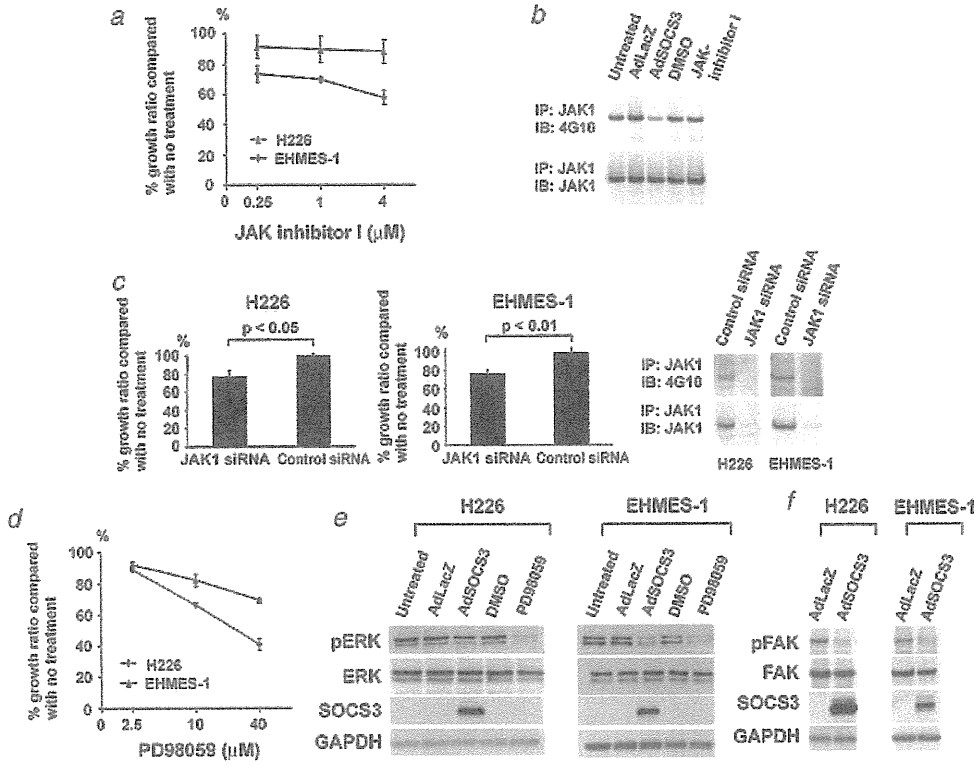

Figure 4. SOCS3 inhibits JAK1, ERK and FAK signaling. (*a*) Growth curves of H226 and EHMES-1 cells treated with JAK inhibitor I. Cells were cultured in RPMI 1640 medium containing 10% FCS with 0.25–4 μM JAK inhibitor I or dimethyl sulfoxide (DMSO) (untreated). After a 3-day culture, viable cell numbers were counted with the MTS assay. Figures show the average (points) of triplicate wells ± SD (bars). (*b*) Inhibition of JAK1 phosphorylation by AdSOCS3. H226 cells were cultured in RPMI 1640 medium containing 0.5% FCS with 1 μM JAK inhibitor I or AdSOCS3 at an MOI of 40. After 24 hr of culturing, 100 ng/mL of IL-6 and 100 ng/mL of sIL-6R were added for 10 min and protein extracts were immunoprecipitated with anti-JAK1 antibody and blotted with antiphosphotyrosine antibody (clone 4G10). (*c*) Growth of H226 and EHMES-1 cells treated with JAK1 siRNA. Cells were treated with either JAK1 siRNA or nonspecific siRNA as control. Cells were cultured in RPMI 1640 medium containing 0.5% FCS, 100 ng/mL of IL-6 and 100 ng/mL of sIL-6R. After a 3-day culture, viable cell numbers were counted with the MTS assay. Figures show the average (columns) of triplicate wells + SD (bars). Protein extracts were immunoprecipitated with anti-JAK1 antibody and blotted with antiphosphotyrosine antibody (clone 4G10) and subsequently with anti-JAK1 antibody. (*d*) Growth curves of H226 and EHMES-1 cells treated with PD98059. Cells were cultured in RPMI 1640 medium containing 10% FCS with 2.5–40 μM PD98059 or dimethyl sulfoxide (DMSO) (untreated). After a 6-day culture, viable cell numbers were counted with the MTS assay. Figures show the average (points) of triplicate wells ± SD (bars). (*e*) Inhibition of ERK phosphorylation by AdSOCS3. H226 and EHMES-1 cells were cultured in RPMI 1640 medium containing 0.5% FCS with 4 μM PD98059 or AdSOCS3 at an MOI of 40. After 24 hr of culturing, protein extracts were blotted with antiphospho-ERK antibody. (*f*) Negative regulation of FAK signaling by SOCS3. H226 and EHMES-1 cells were cultured in RPMI 1640 medium containing 10% FCS with AdSOCS3 at an MOI of 40. After 24 hr of culturing, cells were cultured in RPMI 1640 medium containing 0.5% FCS for an additional 24 hr. Protein extracts were blotted with antiphospho-FAK antibody.

SOCS3 were detected at an MOI of 40 in MPM cells (Figs. 2*b* and 2*c*), we performed subsequent experiments using AdSOCS3 at an MOI of 40.

SOCS3 induces apoptosis and G0/G1 arrest in MPM cells

Next, we investigated the mechanism by which AdSOCS3 inhibited cell growth in H226, EHMES-1, MESO-1 and MESO-4 cells. Since light microscopy findings suggested poor cell viability, apoptosis in these cells was tested by means of annexin V and 7-AAD staining using flow cytometry three days after the addition of AdSOCS3 to the culture. The results of flow cytometric analysis led to the identification of two types of cells: early apoptotic (AnnexinV^+7-AAD^-) and late apoptotic (Annexin V^+7-AAD^+). Compared to treatment with AdLacZ, treatment with AdSOCS3 resulted in elevated

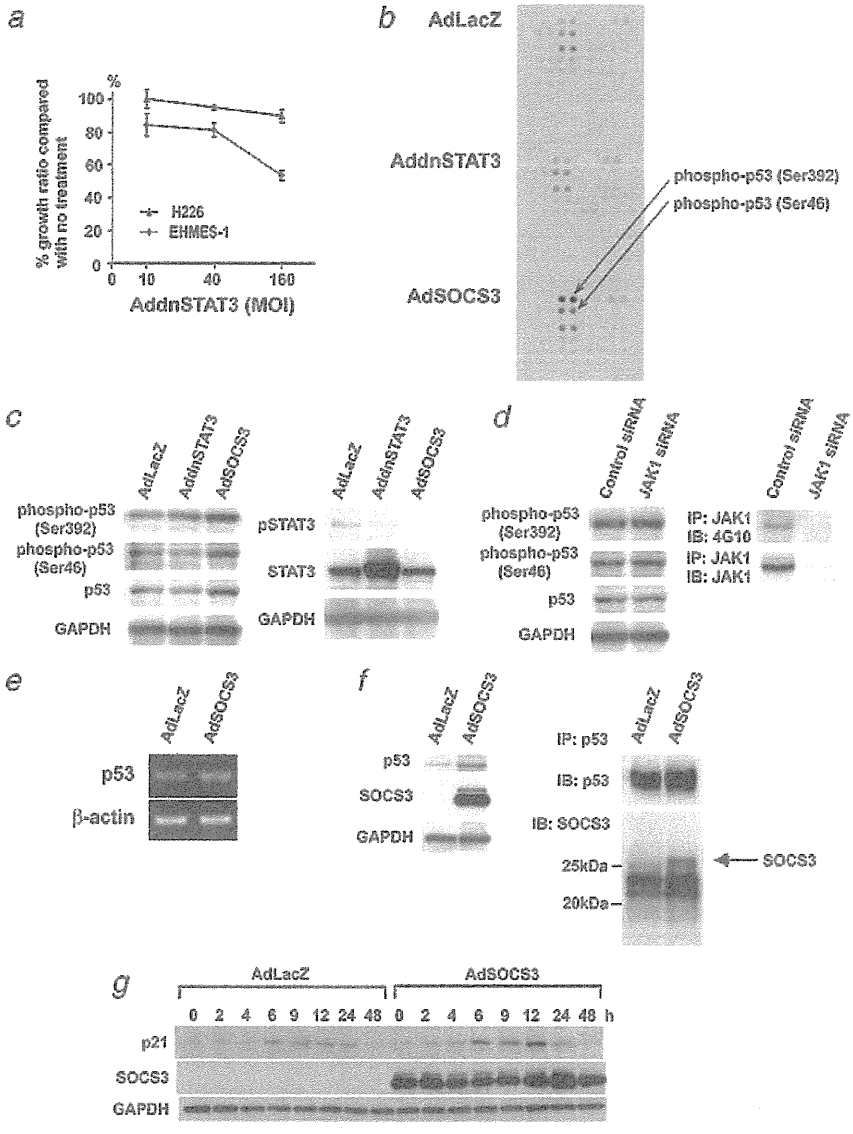

Figure 5. SOCS3 regulates p53 expression in a STAT3-independent manner. (*a*) Growth curves of H226 and EHMES-1 cells treated with AddnSTAT3. Cells were infected with either AddnSTAT3 or AdLacZ as control at an MOI of 10–160. Cells were cultured in RPMI 1640 medium containing 10% FCS. After a 3-day culture, viable cell numbers were counted with the MTS assay. Figures show the average (points) of triplicate wells ± SD (bars). (*b*) Phospho-kinase array revealed that H226 cells treated with AdSOCS3 showed higher levels of phospho-p53 (Ser 392) and phospho-p53 (Ser 46) expression than those treated with AddnSTAT3 or AdLacZ. H226 cells were cultured in RPMI 1640 medium containing 0.5% FCS with AdSOCS3 at an MOI of 40. After 24 hr of culturing, protein extracts were examined with a phospho-kinase array with each phosphorylated protein identified in duplicate. The double-labeled spots in the upper right corner represent the positive controls. (*c*) p53 expression was induced by AdSOCS3. H226 cells were cultured in RPMI 1640 medium containing 0.5% FCS with AdSOCS3 at an MOI of 40. After 24 hr of culturing, protein extracts were probed with antiphospho-p53 (Ser 392), phospho-p53 (Ser 46), p53, phospho-STAT3, STAT3 and GAPDH antibody. (*d*) Influence of JAK1 siRNA on p53 expression. Either JAK1 siRNA or nonspecific siRNA as control was added to H226 cells. Cells were cultured in RPMI 1640 medium containing 0.5% FCS. After 48 hr of culturing, 100 ng/mL of IL-6 and 100 ng/mL of sIL-6R were added for 10 min. The protein extracts were probed with antiphospho-p53 (Ser 392), phospho-p53 (Ser 46), p53 and GAPDH antibody or immunoprecipitated with anti-JAK1 antibody and blotted with antiphosphotyrosine antibody (clone 4G10) and subsequently with anti-JAK1 antibody. (*e*) Expression of p53. RT-PCR was used to determine levels of p53 expression. (*f*) SOCS3 interacts with p53. H226 cells were cultured in RPMI 1640 medium containing 10% FCS with AdSOCS3 at an MOI of 40. After 24 hr of culturing, protein extracts were immunoprecipitated with anti-p53 antibody and immunoblotted with anti-SOCS3 antibody. (*g*) SOCS3 enhances p21 expression. H226 cells were cultured in RPMI 1640 medium containing 10% FCS with AdSOCS3 at an MOI of 40. After 12 hr of culturing, H226 cells were treated with doxorubicin (300 ng/mL) for 0–48 hr. Protein extracts were immunoblotted with anti-p21 antibody.

apoptosis in both early and late apoptotic subsets in H226, EHMES-1, MESO-1 and MESO-4 cells (Fig. 3*a*). Furthermore, cleaved caspase-3, one of the key molecules in apoptosis, was detected in whole cell extracts of H226, EHMES-1, MESO-1 and MESO-4 cells treated with AdSOCS3 (Fig. 3*b*). We therefore conclude that AdSOCS3 induced apoptosis in MPM cells.

In addition to apoptosis, cell cycle regulation is an important mechanism for inhibition of cell growth. To analyze the effect of AdSOCS3 on cell cycle regulation, we infected H226, EHMES-1, MESO-1 and MESO-4 cells with AdSOCS3 and then analyzed cell cycle distribution by means of flow cytometry. When H226 and MESO-4 cells were treated with AdSOCS3, the G0/G1 cell population increased more than in those treated with AdLacZ (Fig. 3*c*).

SOCS3 inhibits JAK1, ERK and FAK signaling

One of the important signaling pathways regulated by SOCS3 is the JAK/STAT3 pathway. We used JAK inhibitor I, which suppresses JAK2 signaling, to investigate the regulation of cell growth by JAK signaling pathways. For this assay, we used H226 and EHMES-1 cell lines (on which MRA had no growth inhibitory effect) to investigate the IL6-independent growth inhibitory effect by SOCS3. As shown in Figure 4*a*, only the growth of EHMES-1 cells, and not of H226 cells, was inhibited by JAK inhibitor I. This suggests that AdSOCS3 inhibited cell growth in H226 cells *via* signaling pathways which were not inhibited by JAK inhibitor I.

To identify the differences between the inhibitory effects of AdSOCS3 and JAK inhibitor I on JAK signaling pathways, we studied changes in the phosphorylation status of JAK1 in H226 cells treated with AdSOCS3 and JAK inhibitor I. Figure 4*b* shows that AdSOCS3 suppressed IL-6–stimulated JAK1 phosphorylation, but that JAK inhibitor I did not affect it. These results lead us to propose that SOCS3 inhibited cell growth in H226 in part by means of negative regulation of JAK1.

We used JAK1 siRNA to evaluate the role of JAK1 signaling pathways in cell growth. As seen in Figure 4*c*, JAK1 siRNA inhibited cell growth in H226 and EHMES-1 cells, suggesting that the growth of H226 cells was partially regulated by JAK1 signaling.

Because it has been reported that SOCS3 inhibits the ERK and FAK signalling pathways, we examined these pathways in H226 and EHMES-1 cells. Figure 4*d* demonstrated that the growth of H226 and EHMES-1 cells was inhibited by the ERK inhibitor PD98059, while ERK phosphorylation was inhibited by AdSOCS3 in these cells (Fig. 4*e*). In addition, AdSOCS3 inhibited phospho-FAK and FAK in H226 and EHMES-1 cells (Fig. 4*f*). We therefore conclude that overexpression of SOCS3 regulates multiple signaling pathways in MPM cells.

SOCS3 regulates p53 expression

We next investigated the role of STAT3 in H226 and EHMES-1 cells and used AddnSTAT3 to examine the regulation of cell growth by STAT3 signaling pathways. As seen in Figure 5*a*, AddnSTAT3 inhibited cell growth in EHMES-1 cells but not in H226 cells. Since this suggests that STAT3 is not involved in the growth of H226 cells, we focused our study on signaling pathways independent of STAT3.

To identify the target molecules of SOCS3 in STAT3-independent pathways, we used a phospho-kinase array to evaluate the expression profile of phosphorylated proteins in H226 cells. Figure 5*b* shows that expression of phospho-p53 (Ser 392) and phospho-p53 (Ser 46) in H226 cells after treatment with AdSOCS3 was higher than in those treated with either AddnSTAT3 or AdLacZ. In addition to phospho-p53, p53 was also highly expressed when treated with AdSOCS3 (Fig. 5*c*). These results suggest that SOCS3 regulated p53 expression.

We next investigated whether JAK1 regulates p53 expression. To this end, we used JAK1 siRNA for the transfection of H226 cells and Western blotting for the examination of p53 expression. As shown in Figure 5*d*, silencing of JAK1 did not influence p53 expression, indicating that JAK1 and p53 are regulated by SOCS3 *via* independent pathways.

Since transfection with AdSOCS3 did not enhance transcription of p53 in H226 cells (Fig. 5*e*), we next investigated whether SOCS3 interacts with p53. After transfection of AdSOCS3 into H226 cells, we detected SOCS3 in the immunoprecipitate of a p53-specific antibody (Fig. 5*f*). In addition, SOCS3 enhanced the expression of p21 which was the target of p53 (Fig. 5*g*). Taken together, these findings suggest that SOCS3 interacts with p53 protein.

SOCS3 exhibits antitumor activity in a mesothelioma xenograft model

We also evaluated the therapeutic effect of AdSOCS3 injection on the growth of subcutaneously or intrathoracically implanted MPM cells in ICR *nu/nu* mice. Of the MPM cell lines used in our study, we were able to establish H226 and MESO-4 xenograft models. Injection of AdSOCS3 vector (1×10^8 pfu/50 μL) intratumorally twice per week reduced tumor volumes compared to tumor volumes in control AdLacZ-injected animals (Fig. 6*a*). Preliminary experiments revealed that when 1×10^6 MPM cells (H226 or MESO-4) were inoculated into the thoracic space, dissemination of tumors was observed in all mice 28 days after cell implantation. Injection of the AdSOCS3 vector (5×10^7 pfu/150 μL) into the thoracic cavity 7, 14 and 21 days after the implantation of 1×10^6 MPM cells (H226 or MESO-4), reduced the weight of tumor nodules compared to the weight of those in control AdLacZ-injected animals (Figs. 6*b* and 6*c*). Finally, Western blot and immunohistochemical analysis indicated that SOCS3 was overexpressed and induced apoptosis in the

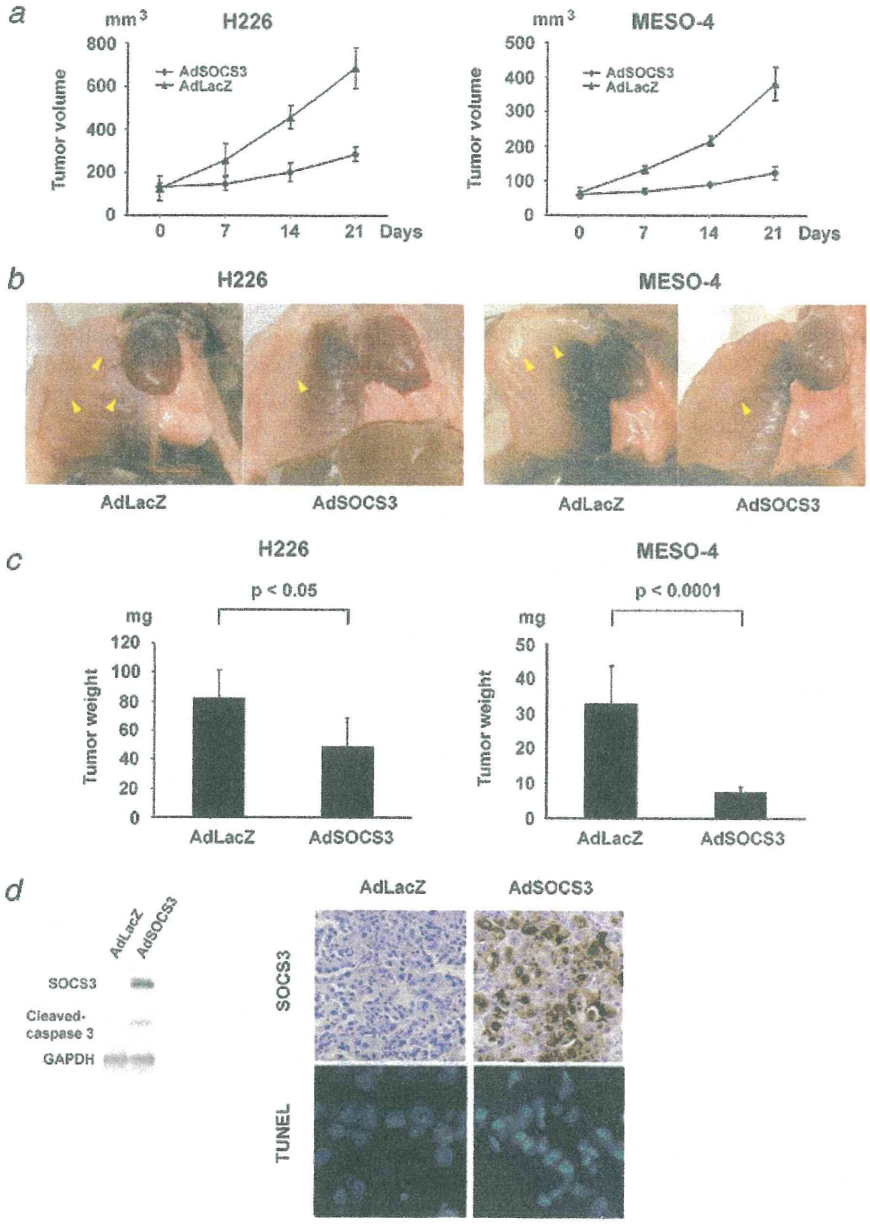

Figure 6. SOCS3 exhibits antitumor activity in a mesothelioma xenograft model. (*a*) Female ICR *nu/nu* mice were intratumorally treated with 1×10^8 pfu of AdSOCS3 or AdLacZ twice per week after the implantation of 3×10^6 H226 or MESO-4 cells subcutaneously in the flank of mice. Tumor volumes were determined weekly. Figures show the average (points) for five animals ± SD (bars). (*b*) Gross appearance of H226 and MESO-4 tumors grown orthotopically in the thoracic spaces. Female ICR *nu/nu* mice were intrathoracically treated with 5×10^7 pfu of AdSOCS3 or AdLacZ for 7, 14 and 21 days after the implantation of 1×10^6 H226 or MESO-4 cells into the pleural space. After 28 days of tumor cell inoculation, the animals were sacrificed and pleural dissemination of the tumor cells was assessed. (*c*) Each tumor nodule found in the thoracic spaces was also weighed. Figures show the average (columns) for eight animals + SD (bars). (*d*) Western blot analysis of SOCS3 and cleaved caspase-3 in H226 tissue from AdSOCS3-injected animals (left panel). The H226 cell bearing animals were treated with AdSOCS3 on day 7 and sacrificed on day 10. The thoracic tumors were analyzed by Western blot. Immunohistochemical analysis of SOCS3 and TUNEL (blue fluorescence = DAPI staining for nuclei; cyan fluorescence = TUNEL positivity) in H226 tissue from AdSOCS3-injected animals (right panel). The animals were treated in the same way as described above.

H226 tissue from AdSOCS3-injected animals (Fig. 6*d*). Immunohistochemical analysis of SOCS3 overexpression and apoptosis in MESO-4 tissue could not be clearly determined, however Western blot analysis showed identical results to that observed in H226 tissue (data not shown). From these results, we conclude that SOCS3 exhibits antitumor activity not only *in vitro* but also *in vivo* in the MPM model. We hope that these findings may lead to the successful clinical application of SOCS3 for MPM treatment.

Discussion

Malignant mesothelioma represents a great challenge to both clinicians and researchers due to its poor prognosis and remarkable resistance to current therapies. Although there have been some improvements in treatment over the past few years, a better understanding of the molecular basis of the disease and of how to improve treatment is required. Among molecular targeted therapies, recently developed tyrosine kinase inhibitors have been tested for MPM but without therapeutic benefit. This is partially explained by the fact that multiple receptor tyrosine kinases are frequently activated in most MM cells.[23] In our study, we showed that SOCS3 inhibited the proliferation of MPM cells through multiple signaling pathways including JAK/STAT3, ERK, FAK and p53 pathways. We observed that SOCS3 did not influence the expression and activation of p38, JNK, Akt or GSK3β proteins in H226 and EHMES-1 cell lines (data not shown). Specifically, we were able to demonstrate that AdSOCS3 inhibits MPM progression in a mouse pleural xenograft model. These data provide new insights into the clinical application of SOCS3 gene delivery for the treatment of MPM.

We also provided evidence that MRA had little effect on proliferation of MPM cells. A recent study by Adachi *et al.*[12] found that MRA is capable of blocking IL-6 signaling and suppresses the cell growth of MPM induced by IL-6/sIL-6R. We hypothesize that MRA was not able to inhibit proliferation of these cells because it did not inhibit signals from other cytokines acting through gp130 or endogenous activated molecules downstream of gp130 involved in proliferation of these cells.

There are several JAK inhibitors, including JAK inhibitor I,[33] but these inhibitors inhibit JAK1 less than they do other JAK family molecules. This may explain why, although JAK1 is involved in H226 cell proliferation, JAK inhibitor I had little effect on proliferation of H226 cells. SOCS3, however, is an effective JAK1 inhibitory molecule and also inhibits proliferation of H226 cells. It has further been reported that JAK2 inhibitors have antitumor effects on various cancer cells.[34] Because of its pan-JAK inhibitory effect,[20] SOCS3 appears to be a promising antitumor molecule.

We were able to show that SOCS3 regulated phospho-p53 (Ser392 and Ser46) and total p53 expression. Functional inactivation of the p53 pathways appears to be a critical requirement for the development of several human cancers.[35] In spite of the fact that mutations in p53 are among the most commonly acquired genetic lesions seen in cancers, p53 mutations are rarely seen in MPM including H226 cells.[36] It has been reported that Ser392 phosphorylation may regulate the oligomerization of p53 and thus its sequence-specific DNA binding,[37,38] while phosphorylation of Ser46 has been implicated in the activation of p53-dependent apoptotic responses.[39,40] The most thoroughly characterized downstream target of p53 activation is the induction of p21 expression, with p21 playing a critical role in the cell cycle checkpoint.[41] In our study, moreover, SOCS3 enhanced p21 expression and induced apoptosis and G0/G1 arrest in MPM cells. In view of these results, we propose that SOCS3 induces apoptosis as well as G0/G1 arrest partially through the p53 pathways in MPM cells.

Recently, it has been reported that SOCS1 activates p53 *via* a direct interaction between the SH2 domain of SOCS1 and the N-terminal transactivation domain of p53,[42] while we were able to show that SOCS3 did not enhance transcription of p53 but interacted with p53. It is thus conceivable that the observed interaction of SOCS3 with p53 may in turn enhance p53 protein stability. Such a mechanism may therefore involve the inhibition of interaction of p53 with other proteins that promote p53 protein degradation.

In our study, we used adenoviral SOCS3 gene transfer to the thoracic cavity in a mouse xenograft pleural tumor model to provide evidence of a potent antitumor effect of SOCS3 *in vivo*. Because MPM locates within the thoracic cavity and rarely displays widespread metastasis, gene transfer to the thoracic cavity makes this tumor uniquely accessible, thus facilitating the direct administration of novel therapeutic agents and subsequent analysis of treatment effects. Clinical trials involving intrapleural administration of adenoviral vectors to MPM patients have demonstrated that intrapleural gene therapy using adenoviral vectors is safe and well tolerated by MPM patients.[43,44]

In conclusion, we demonstrated the antitumor effect of SOCS3 against MPM both *in vitro* and *in vivo*. The results of clinical application of SOCS3 for MPM treatment are eagerly anticipated.

Acknowledgements

This work was supported by a Grant-in-Aid from the Ministry of Health, Labour and Welfare, Japan (T. Naka), a Grant-in-Aid for Young Scientists (B) from the Ministry of Education, Culture, Sports, Science and Technology, Japan (K. Iwahori) and a grant from the Kansai Biomedical Cluster Project in Saito, which is promoted by the Knowledge Cluster Initiative of the Ministry of Education, Culture, Sports, Science and Technology, Japan (T. Naka). We wish to thank Akihito Yokoyama (Kochi University, Kochi, Japan) and Hironobu Hamada (Ehime University, Ehime, Japan) for providing helpful comments on this article, and Namiko Kawakami and Yukako Ito for their secretarial assistance.

References

1. Vogelzang NJ, Rusthoven JJ, Symanowski J, Denham C, Kaukel E, Ruffie P, Gatzemeier U, Boyer M, Emri S, Manegold C, Niyikiza C, Paoletti P. Phase III study of pemetrexed in combination with cisplatin versus cisplatin alone in patients with malignant pleural mesothelioma. *J Clin Oncol* 2003;21:2636–44.
2. Pelucchi C, Malvezzi M, La Vecchia C, Levi F, Decarli A, Negri E. The Mesothelioma epidemic in Western Europe: an update. *Br J Cancer* 2004;90: 1022–4.
3. Leigh J, Driscoll T. Malignant mesothelioma in Australia, 1945–2002. *Int J Occup Environ Health* 2003;9:206–17.
4. Leithner K, Leithner A, Clar H, Weinhaeusel A, Radl R, Krippl P, Rehak P, Windhager R, Haas OA, Olschewski H. Mesothelioma mortality in Europe: impact of asbestos consumption and simian virus 40. *Orphanet J Rare Dis* 2006;1:44.
5. Murayama T, Takahashi K, Natori Y, Kurumatani N. Estimation of future mortality from pleural malignant mesothelioma in Japan based on an age-cohort model. *Am J Ind Med* 2006;49:1–7.
6. Fitzpatrick DR, Peroni DJ, Bielefeldt-Ohmann H. The role of growth factors and cytokines in the tumorigenesis and immunobiology of malignant mesothelioma. *Am J Respir Cell Mol Biol* 1995;12:455–60.
7. Galffy G, Mohammed KA, Dowling PA, Nasreen N, Ward MJ, Antony VB. Interleukin 8: an autocrine growth factor for malignant mesothelioma. *Cancer Res* 1999;59:367–71.
8. Lee TC, Zhang Y, Aston C, Hintz R, Jagirdar J, Perle MA, Burt M, Rom WN. Normal human mesothelial cells and mesothelioma cell lines express insulin-like growth factor I and associated molecules. *Cancer Res* 1993;53:2858–64.
9. Morocz IA, Schmitter D, Lauber B, Stahel RA. Autocrine stimulation of a human lung mesothelioma cell line is mediated through the transforming growth factor alpha/epidermal growth factor receptor mitogenic pathway. *Br J Cancer* 1994;70: 850–6.
10. Versnel MA, Claesson-Welsh L, Hammacher A, Bouts MJ, van der Kwast TH, Eriksson A, Willemsen R, Weima SM, Hoogsteden HC, Hagemeijer A, et al. Human malignant mesothelioma cell lines express PDGF beta-receptors whereas cultured normal mesothelial cells express predominantly PDGF alpha-receptors. *Oncogene* 1991;6:2005–11.
11. Monti G, Jaurand MC, Monnet I, Chretien P, Saint-Etienne L, Zeng L, Portier A, Devillier P, Galanaud P, Bignon J, et al. Intrapleural production of interleukin 6 during mesothelioma and its modulation by gamma-interferon treatment. *Cancer Res* 1994;54:4419–23.
12. Adachi Y, Aoki C, Yoshio-Hoshino N, Takayama K, Curiel DT, Nishimoto N. Interleukin-6 induces both cell growth and VEGF production in malignant mesotheliomas. *Int J Cancer* 2006;119: 1303–11.
13. Buettner R, Mora LB, Jove R. Activated STAT signaling in human tumors provides novel molecular targets for therapeutic intervention. *Clin Cancer Res* 2002;8: 945–54.
14. Endo TA, Masuhara M, Yokouchi M, Suzuki R, Sakamoto H, Mitsui K, Matsumoto A, Tanimura S, Ohtsubo M, Misawa H, Miyazaki T, Leonor N, et al. A new protein containing an SH2 domain that inhibits JAK kinases. *Nature* 1997;387: 921–4.
15. Naka T, Narazaki M, Hirata M, Matsumoto T, Minamoto S, Aono A, Nishimoto N, Kajita T, Taga T, Yoshizaki K, Akira S, Kishimoto T. Structure and function of a new STAT-induced STAT inhibitor. *Nature* 1997;387:924–9.
16. Starr R, Willson TA, Viney EM, Murray LJ, Rayner JR, Jenkins BJ, Gonda TJ, Alexander WS, Metcalf D, Nicola NA, Hilton DJ. A family of cytokine-inducible inhibitors of signalling. *Nature* 1997;387: 917–21.
17. Rakesh K, Agrawal DK. Controlling cytokine signaling by constitutive inhibitors. *Biochem Pharmacol* 2005;70: 649–57.
18. Naka T, Fujimoto M, Tsutsui H, Yoshimura A. Negative regulation of cytokine and TLR signalings by SOCS and others. *Adv Immunol* 2005;87:61–122.
19. Yoshimura A, Naka T, Kubo M. SOCS proteins, cytokine signalling and immune regulation. *Nat Rev Immunol* 2007;7: 454–65.
20. Nicholson SE, De Souza D, Fabri LJ, Corbin J, Willson TA, Zhang JG, Silva A, Asimakis M, Farley A, Nash AD, Metcalf D, Hilton DJ, et al. Suppressor of cytokine signaling-3 preferentially binds to the SHP-2-binding site on the shared cytokine receptor subunit gp130. *Proc Natl Acad Sci USA* 2000;97:6493–8.
21. He B, You L, Uematsu K, Zang K, Xu Z, Lee AY, Costello JF, McCormick F, Jablons DM. SOCS-3 is frequently silenced by hypermethylation and suppresses cell growth in human lung cancer. *Proc Natl Acad Sci USA* 2003;100: 14133–8.
22. Bromberg J. Stat proteins and oncogenesis. *J Clin Invest* 2002;109:1139–42.
23. Sekido Y. Genomic abnormalities and signal transduction dysregulation in malignant mesothelioma cells. *Cancer Sci* 2010;101:1–6.
24. Poulikakos PI, Xiao GH, Gallagher R, Jablonski S, Jhanwar SC, Testa JR. Re-expression of the tumor suppressor NF2/merlin inhibits invasiveness in mesothelioma cells and negatively regulates FAK. *Oncogene* 2006;25: 5960–8.
25. Lehmann U, Schmitz J, Weissenbach M, Sobota RM, Hortner M, Friederichs K, Behrmann I, Tsiaris W, Sasaki A, Schneider-Mergener J, Yoshimura A, Neel BG, et al. SHP2 and SOCS3 contribute to Tyr-759-dependent attenuation of interleukin-6 signaling through gp130. *J Biol Chem* 2003;278:661–71.
26. Liu E, Cote JF, Vuori K. Negative regulation of FAK signaling by SOCS proteins. *EMBO J* 2003;22:5036–46.
27. Niwa Y, Kanda H, Shikauchi Y, Saiura A, Matsubara K, Kitagawa T, Yamamoto J, Kubo T, Yoshikawa H. Methylation silencing of SOCS-3 promotes cell growth and migration by enhancing JAK/STAT and FAK signalings in human hepatocellular carcinoma. *Oncogene* 2005; 24:6406–17.
28. Miyake S, Makimura M, Kanegae Y, Harada S, Sato Y, Takamori K, Tokuda C, Saito I. Efficient generation of recombinant adenoviruses using adenovirus DNA-terminal protein complex and a cosmid bearing the full-length virus genome. *Proc Natl Acad Sci USA* 1996;93: 1320–4.
29. Kijima T, Osaki T, Nishino K, Kumagai T, Funakoshi T, Goto H, Tachibana I, Tanio Y, Kishimoto T. Application of the Cre recombinase/loxP system further enhances antitumor effects in cell type-specific gene therapy against carcinoembryonic antigen-producing cancer. *Cancer Res* 1999;59: 4906–11.
30. Goto H, Osaki T, Kijima T, Nishino K, Kumagai T, Funakoshi T, Kimura H, Takeda Y, Yoneda T, Tachibana I, Hayashi S. Gene therapy utilizing the Cre/loxP system selectively suppresses tumor growth of disseminated carcinoembryonic antigen-producing cancer cells. *Int J Cancer* 2001; 94:414–9.
31. Nishino K, Osaki T, Kumagai T, Kijima T, Tachibana I, Goto H, Arai T, Kimura H, Funakoshi T, Takeda Y, Tanio Y, Hayashi S. Adenovirus-mediated gene therapy specific for small cell lung cancer cells using a Myc-Max binding motif. *Int J Cancer* 2001;91:851–6.
32. Kanegae Y, Makimura M, Saito I. A simple and efficient method for purification of

infectious recombinant adenovirus. *Jpn J Med Sci Biol* 1994;47:157–66.
33. Lipka DB, Hoffmann LS, Heidel F, Markova B, Blum MC, Breitenbuecher F, Kasper S, Kindler T, Levine RL, Huber C, Fischer T. LS104, a non-ATP-competitive small-molecule inhibitor of JAK2, is potently inducing apoptosis in JAK2V617F-positive cells. *Mol Cancer Ther* 2008;7:1176–84.
34. Verstovsek S, Manshouri T, Quintas-Cardama A, Harris D, Cortes J, Giles FJ, Kantarjian H, Priebe W, Estrov Z. WP1066, a novel JAK2 inhibitor, suppresses proliferation and induces apoptosis in erythroid human cells carrying the JAK2 V617F mutation. *Clin Cancer Res* 2008;14:788–96.
35. Vazquez A, Bond EE, Levine AJ, Bond GL. The genetics of the p53 pathway, apoptosis and cancer therapy. *Nat Rev Drug Discov* 2008;7:979–87.
36. Yonesaka K, Tamura K, Kurata T, Satoh T, Ikeda M, Fukuoka M, Nakagawa K. Small interfering RNA targeting survivin sensitizes lung cancer cell with mutant p53 to adriamycin. *Int J Cancer* 2006;118: 812–20.
37. Sakaguchi K, Sakamoto H, Lewis MS, Anderson CW, Erickson JW, Appella E, Xie D. Phosphorylation of serine 392 stabilizes the tetramer formation of tumor suppressor protein p53. *Biochemistry* 1997; 36:10117–24.
38. Hao M, Lowy AM, Kapoor M, Deffie A, Liu G, Lozano G. Mutation of phosphoserine 389 affects p53 function in vivo. *J Biol Chem* 1996;271:29380–5.
39. D'Orazi G, Cecchinelli B, Bruno T, Manni I, Higashimoto Y, Saito S, Gostissa M, Coen S, Marchetti A, Del Sal G, Piaggio G, Fanciulli M, et al. Homeodomain-interacting protein kinase-2 phosphorylates p53 at Ser 46 and mediates apoptosis. *Nat Cell Biol* 2002;4:11–9.
40. Saito S, Goodarzi AA, Higashimoto Y, Noda Y, Lees-Miller SP, Appella E, Anderson CW. ATM mediates phosphorylation at multiple p53 sites, including Ser(46), in response to ionizing radiation. *J Biol Chem* 2002; 277:12491–4.
41. Abbas T, Dutta A. p21 in cancer: intricate networks and multiple activities. *Nat Rev Cancer* 2009;9:400–14.
42. Calabrese V, Mallette FA, Deschenes-Simard X, Ramanathan S, Gagnon J, Moores A, Ilangumaran S, Ferbeyre G. SOCS1 links cytokine signaling to p53 and senescence. *Mol Cell* 2009;36:754–67.
43. Sterman DH, Recio A, Carroll RG, Gillespie CT, Haas A, Vachani A, Kapoor V, Sun J, Hodinka R, Brown JL, Corbley MJ, Parr M, et al. A phase I clinical trial of single-dose intrapleural IFN-beta gene transfer for malignant pleural mesothelioma and metastatic pleural effusions: high rate of antitumor immune responses. *Clin Cancer Res* 2007;13: 4456–66.
44. Sterman DH, Recio A, Vachani A, Sun J, Cheung L, DeLong P, Amin KM, Litzky LA, Wilson JM, Kaiser LR, Albelda SM. Long-term follow-up of patients with malignant pleural mesothelioma receiving high-dose adenovirus herpes simplex thymidine kinase/ganciclovir suicide gene therapy. *Clin Cancer Res* 2005;11:7444–53.

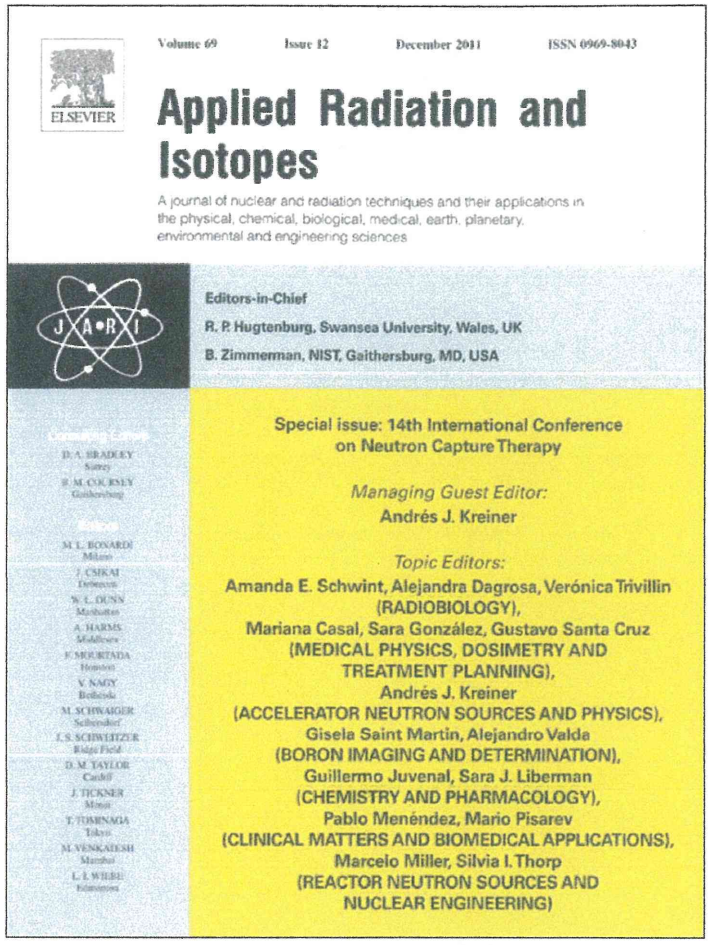

Applied Radiation and Isotopes 69 (2011) 1768–1770

Contents lists available at ScienceDirect

Applied Radiation and Isotopes

journal homepage: www.elsevier.com/locate/apradiso

Synthesis of optically active dodecaborate-containing L-amino acids for BNCT

Shintaro Kusaka [a], Yoshihide Hattori [a,*], Kouki Uehara [b], Tomoyuki Asano [b], Shinji Tanimori [a], Mitsunori Kirihata [a]

[a] Department of Bioscience and Informatics, Graduate School of Life and Environmental Sciences, Osaka Prefecture University, 1-1 Gakuen-cho, Nakaku, Sakai, Japan
[b] Stella Pharma Corporation, ORIX Kouraibashi Bldg. 5F 3-2-7 Kouraibashi, Chuo-ku, Osaka, Japan

ARTICLE INFO

Available online 8 April 2011

Keywords:
Boron cluster containing L-α-amino acid
Dodecaboratethio-L-amino acid
New boron amino acid for BNCT

ABSTRACT

A convenient and simple synthetic method of dodecaboratethio-L-amino acid, a new class of tumor-seeking boron carrier for BNCT, was accomplished from *S*-cyanoethylthioundecahydro-*closo*-dodecaborate (*S*-cyanoethyl-^{10}BSH, $[^{10}B_{12}H_{11}]^{2-}SCH_2CH_2CN$) and bromo-L-α-amino acids by nearly one step *S*-alkylation. An improved synthesis of *S*-cyanoethyl-^{10}BSH, a key starting compound for *S*-alkylation, was also performed by Michael addition of ^{10}BSH with acryronitrile in high yield. Four kinds of new dodecaboratethio-L-amino acids were obtained in optically pure form without the need for any optical resolution.

1. Introduction

Boron-containing L-amino acids are worthwhile synthetic targets due to their potential biological activities, particularly with respect to the boron-neutron capture therapy (BNCT). In many tumor tissues, L-amino acid transport is enhanced to guarantee the multiplication of tumor cells compared with normal tissues (Endou and Kanai, 1999). Therefore, various boron-containing α-amino acids that are closely similar in structure to the usual amino acid such as *p*-boronophenylalanine (BPA) and *o*-carboranyl-glycine, have been synthesized and evaluated (Varadarajan and Hawthorne, 1991; Srivastsva et al., 1997). However, such boron-containing amino acids have low water-solubility associated with poor bioavailability as disadvantages.

Recently, Gabel et al. reported that the synthesis of a new class of water soluble α-amino acids in racemic states, which contained the dianionic dodecaboratethio ($[^{10}B_{12}H_{11}]^{2-}$-S-) unit from undecahydro-*closo*-dodecaborate (BSH) by stepwise alkylation using bromoalkyl-*N*-aceto-amidomalonate derivatives followed by decarboxylation and hydrolytic deprotection (Slepukhina and Gabel, 2006). However, these methods have not been entirely satisfactory, particularly for large amount preparation owing to multiple steps, and for racemic form of the target amino acids.

Here, we describe an efficient route for the simple synthesis of optically pure dodecaboratethio-L-amino acids **1–4** (Fig. 1) as illustrated in the schemes.

2. Material and method

2.1. General

^{1}H NMR spectra were measured on a JMTC-400/54/SS (400 MHz, JEOL Ltd., Tokyo, Japan) spectrometer. The chemical shifts in ^{1}H NMR are given in δ values from TMS used as internal standard. Optical rotations were measured on a Jasco P-2200 polarimeter (JASCO Co., Tokyo, Japan). Electron spray ionization time of flight mass spectra (ESI-TOF MS) was obtained on a Nanofrontier LD (Hitachi High-Technologies Corporation, Tokyo, Japan). ^{10}BSH was provided by Stella Pharma Corporation (Osaka, Japan).

2.2. Synthesis of bis-tetramethylammmonium S-(cyanoethyl)-thioundecahydro-closo-dodecaborate (2) by Michael addition

To a solution of ^{10}BSH.2NMe$_4$ (1.00 g, 3.20 mmol) and 1N NaOH aq. (3.20 mL, 3.20 mmol) in H_2O (20 mL) was added acrylonitrile (255 mg, 4.80 mmol) at room temperature. After stirring for 3 h, the reaction mixture was washed with EtOAc (20 mL × 3), and the aqueous layer was concentrated in vacuo. The residual solid was recrystallized from H_2O to give **2** as colorless crystal (1.08 g, 92%): mp 280–285 °C, ^{1}H NMR (400 MHz, D_2O) δ 0.7–1.5 (11H, m, $^{10}B_{12}H_{11}$), 2.56 (2H, m, $CNCH_2CH_2S$-), 2.65 (2H, m, $CNCH_2CH_2S$-), 3.10 (24H, s, $-N^+(CH_3)_4$).

2.3. Synthesis of dodecaboratethio-L-amino acids (1a–d)

The mixture of bis-tetramethylammmonium *S*-(cyanoethyl)thio-undecahydro-*closo*-dodecaborate (**2**, 0.27 mmol) and ω-bromo-L-amino acids **3a–d** (0.41 mmol) in dry MeCN (7 mL) under argon atmosphere was refluxed for 12 h, and the reaction mixture was

* Corresponding author.
E-mail address: y0shi_hattori@riast.osakafu-u.ac.jp (Y. Hattori).

0969-8043/$ - see front matter © 2011 Elsevier Ltd. All rights reserved.
doi:10.1016/j.apradiso.2011.03.042

concentrated in vacuo. The residual solid was suspended in acetone (30 mL), and the suspension was filtrated by suction to remove the insoluble solid. To the filtrate was added 10% tetramethylammonium hydroxide in MeOH (0.28 mmol) at 0 °C, and the mixture was stirred for 30 min at the same temperature. The collected precipitate by filtration was washed quickly with acetone (30 mL). After dissolving with water, the aqueous solution was passed through an ion-exchange column (Amberlite IR-120, H^+ form). The neutralized filtrate with NaOH was chromatographed using of ODS column to give pure dodecaboratelthio-L-amino acids **1a–d**.

2.3.1. (R)-2-Amino-3-(dodecaboranylthio)pro-panoic acid disodium salt (1a)

^{1}H NMR (D_2O); 0.75–1.80 (11H, m, $^{10}B_{12}H_{11}$), 2.52–2.66 (2H, m, 3-CH_2), 3.80 (1H, m, 2-CH); ESI-TOF MS (neg.): found m/z 274.5 $[M+Na]^-$ (calcd. for $C_3H_{17}{}^{10}B_{12}NO_2S$+Na: 274.2).

2.3.2. (S)-2-Amino-4-(dodecaboranylthio)butyric acid disodium salt (1b)

^{1}H NMR (D_2O); 0.75–1.60 (11H, m, $^{10}B_{12}H_{11}$), 1.91–2.03 (2H, m, 3-CH_2), 2.43 (2H, m, 4-CH_2), 3.62 (1H, m, 2-CH); $[\alpha]_D^{25}$ −1.93 (*c* 0.505, H_2O); ESI-TOF MS (neg.): found m/z 288.2 $[M+Na]^-$ (calcd. for $C_4H_{19}{}^{10}B_{12}NO_2S$+Na: 288.3).

2.3.3. (S)-2-Amino-5-(dodecaboranylthio)pentanoic acid disodium salt (1c)

^{1}H NMR (D_2O); 0.75–1.50 (11H, m, $^{10}B_{12}H_{11}$), 1.50 (2H, m, 4-CH_2), 1.60–1.80 (2H, m, 3-CH_2), 2.37 (2H, m, 5-CH_2), 3.30 (1H, m, 2-CH); $[\alpha]_D^{25}$ −2.06 (*c* 0.515, H_2O); ESI-TOF MS (neg.): found m/z 302.6 $[M+Na]^-$ (calcd. for $C_5H_{21}{}^{10}B_{12}NO_2S$+Na: 302.3).

2.3.4. (S)-2-Amino-5-(dodecaboranylthio)oc-tanoic acid disodiumsalt (1d)

^{1}H NMR (D_2O); 0.75–1.60 (11H, m, $^{10}B_{12}H_{11}$), 1.21–1.41(4H, m, 4-CH_2, 5-CH_2), 1.41 (2H, m, -6-CH_2), 1.70(4H, m, 3-CH_2-, 7-CH_2), 2.34 (2H, t, J=7.3 Hz, 8-CH_2), 3.57(1H, m, 2-CH); $[\alpha]_D^{25}$ −1.96 (*c* 0.515, H_2O); ESI-TOF MS (neg.): found m/z 344.5 $[M+Na]^-$ (calcd. for $C_8H_{27}{}^{10}B_{12}NO_2S$+Na: 344.3).

3. Results and discussion

In our initial attempt we employed direct alkylation of ^{10}BSH with ω-bromo-L-amino acid to prepare mono-*S*-alkyl^{10}BSH, however, the inseparable mixture of mono- and di-*S*-alkyl adducts were invariably formed. After several unsuccessful trials, we employed stepwise alkylation method using *S*-cyanoethyl-^{10}BSH (**2**), a key intermediate in this synthesis, according to the reported method (Gabel et al., 1993).

Gabel et al. have reported the stepwise synthesis of *S*-cyanoethyl-^{10}BSH (**2**), a useful intermediate for alkylation, stating from ^{10}BSH and bromo-propionitrile by two steps sequence. However, the overall yields were unsatisfactory.

We devised more efficient synthetic route based on hetero Michael reaction as shown in Scheme 1–3. Thus, ^{10}BSH was treated with acrylonitrile in aqueous solution using sodium hydroxide as a base to give pure *S*-cyanoethyl-^{10}BSH (**2**) as solid in 88% yields.

On the other hand, ω-bromo-L-amino acids (**3a–d**), represented as Br-(CH_2)n-CH(NH_2)COOH (n=1, 2, 3, 6), were prepared as hydrochloric or hydrobromic salts. Among them, (*S*)-2-amino-4-bromobutyric acid (**3b**, n=2) was commercially purchased, and other ω-bromo-L-amino acids bearing (*L*)-configuration were obtained

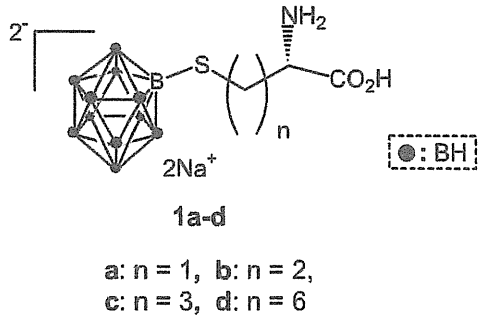

Fig. 1. Dodecaboratethio-L-amino acids.

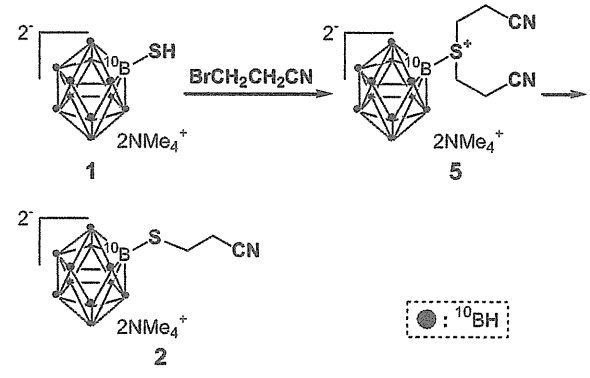

Scheme 2. Stepwise synthesis of *S*-cyanoethyl BSH by alkylation.

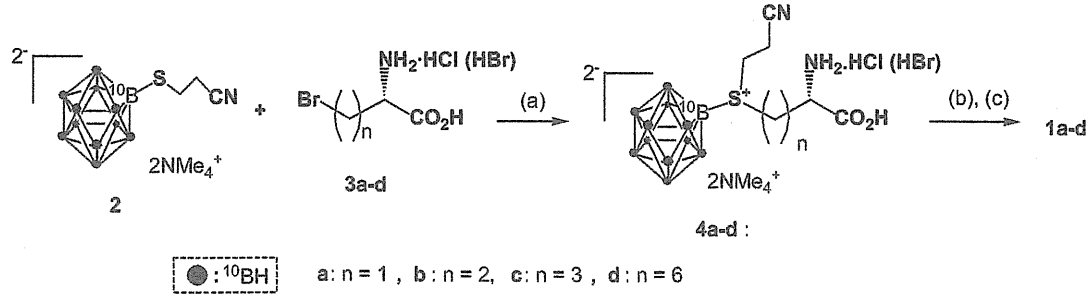

Reagents and conditions: a) MeCN, reflux, 24h, b) Me_4NOH, $MeNH_2$, acetone, r.t., 30 min, c) amberlite IR-120 (Na+)

Scheme 1. Simple and efficient synthesis of dodecaboratethio -L-amino acids (**1a–d**).